Climate response of direct radiative forcing of anthropogenic black carbon

Serena H. Chung

Cooperative Institute for Research in Environmental Sciences, Boulder, Colorado, USA

Aeronomy Laboratory, National Oceanic and Atmospheric Administration, Boulder, Colorado, USA

John H. Seinfeld

Departments of Chemical Engineering and Environmental Science and Engineering, California Institute of Technology, Pasadena, California, USA

Received 15 September 2004; revised 10 March 2005; accepted 17 March 2005; published 1 June 2005.

[1] The equilibrium climate effect of direct radiative forcing of anthropogenic black carbon (BC) is examined by 100-year simulations in the Goddard Institute for Space Studies General Circulation Model II-prime coupled to a mixed-layer ocean model. Anthropogenic BC is predicted to raise globally and annually averaged equilibrium surface air temperature by 0.20 K if BC is assumed to be externally mixed. The predicted increase is significantly greater in the Northern Hemisphere (0.29 K) than in the Southern Hemisphere (0.11 K). If BC is assumed to be internally mixed with the present-day level of sulfate aerosol, the predicted annual mean surface temperature increase rises to 0.37 K globally, 0.54 K for the Northern Hemisphere, and 0.20 K for the Southern Hemisphere. The climate sensitivity of BC direct radiative forcing is calculated to be 0.6 K W^{-1} m^2, which is about 70% of that of CO_2, independent of the assumption of BC mixing state. The largest surface temperature response occurs over the northern high latitudes during winter and early spring. In the tropics and midlatitudes, the largest temperature increase is predicted to occur in the upper troposphere. Direct radiative forcing of anthropogenic BC is also predicted to lead to a change of precipitation patterns in the tropics; precipitation is predicted to increase between 0 and 20°N and decrease between 0 and 20°S, shifting the intertropical convergence zone northward. If BC is assumed to be internally mixed with sulfate instead of externally mixed, the change in precipitation pattern is enhanced. The change in precipitation pattern is not predicted to alter the global burden of BC significantly because the change occurs predominantly in regions removed from BC sources.

Citation: Chung, S. H., and J. H. Seinfeld (2005), Climate response of direct radiative forcing of anthropogenic black carbon, *J. Geophys. Res.*, *110*, D11102, doi:10.1029/2004JD005441.

1. Introduction

[2] Atmospheric abundances of tropospheric greenhouse gases (GHGs) and aerosols have increased since the preindustrial period due to anthropogenic activities, and are estimated to make significant contributions to perturbing the radiative balance of the Earth-atmosphere system over the next century [*Houghton et al.*, 2001]. While GHGs such as CO_2 and CH_4 warm the atmosphere by trapping outgoing infrared radiation, anthropogenic aerosols, such as sulfates or black carbon (BC), cool or warm the atmosphere by scattering or absorbing solar radiation, respectively. Among radiatively active species of anthropogenic origin in the atmosphere, BC is increasingly recognized as an important contributer to global climate change [*Jacobson*, 2002; *Hansen and Nazarenko*, 2004; *Roberts and Jones*, 2004; *Wang*, 2004]. Anthropogenic BC is also considered an important factor in the perturbation of regional climate [*Ramanathan et al.*, 2001a, 2001b; *Menon et al.*, 2002].

[3] The first-order estimate of the climate impact of an atmospheric constituent is the direct radiative forcing it induces, which measures the net change in incoming and outgoing irradiance, usually calculated at top of the atmosphere (TOA) or at the tropopause. The concept of radiative forcing as a measure of climate change is justified by the assumption that, for small perturbations, the equilibrium global and annual mean surface air temperature change ($\Delta[\bar{T}_s]$) is approximately linearly related to the global and annual mean radiative forcing ($\Delta[\bar{F}]$), i.e.,

$$\Delta[\bar{T}_s] = \lambda \Delta[\bar{F}], \tag{1}$$

where λ is the climate sensitivity in units of K W^{-1} m^2. Indeed, climate model experiments have shown that, for relatively spatially homogeneous radiative forcing, λ is

0148-0227/05/2004JD005441$09.00

reasonably independent of the nature of the forcing within an individual climate model (within 20%). For example, *Hansen et al.* [1984, 1997], *Forster et al.* [2000], and *Joshi et al.* [2003], show that the climate responses for doubled CO_2 and a 2% increase in solar irradiance are remarkably similar even though solar forcing affects shortwave radiation and CO_2 mainly affects longwave radiation.

[4] An important factor in the linear relationship of equation (1) is that $\Delta[\bar{F}]$ needs to be defined appropriately. The IPCC Assessment [*Houghton et al.*, 2001] defines radiative forcing as the "change in net (down minus up) irradiance (solar plus longwave; in W m^{-2}) at the tropopause AFTER allowing for stratospheric temperatures to readjust to radiative equilibrium, but with surface and tropospheric temperature and state held fixed at the unperturbed values." The rationale for using this adjusted (instead of instantaneous) forcing is that the radiative relaxation time of the stratosphere is a few weeks, much faster than the decadal timescale for the surface-troposphere system, which is governed by the thermal inertial of the ocean [*Hansen et al.*, 1997; *Shine and Forster*, 1999]. Because radiative forcing for tropospheric aerosols is normally reported in the literature as the instantaneous forcing at TOA, unless otherwise noted, forcings for aerosols reported in this study are instantaneous direct radiative forcings at TOA. Note that for tropospheric aerosols that only interact with shortwave radiation, such as sulfate and BC, the instantaneous forcing at TOA, instantaneous forcing at tropopause, and adjusted forcing at tropopause are approximately equal [*Hansen et al.*, 1997]; therefore, no accuracy is lost in using the instantaneous forcing instead of the adjusted forcing for BC or sulfate.

[5] Global annual mean adjusted direct radiative forcing at the tropopause of CO_2 and other GHGs has been estimated at +2.43 W m^{-2} [*Houghton et al.*, 2001]. For BC, the estimate (at TOA) ranges from +0.16 to +0.80 W m^{-2} [*Haywood and Shine*, 1995; *Haywood et al.*, 1997; *Haywood and Ramaswamy*, 1998; *Myhre et al.*, 1998; *Penner et al.*, 1998; *Cooke et al.*, 1999; *Jacobson*, 2000; *Koch*, 2001; *Chung and Seinfeld*, 2002; *Wang*, 2004]. The differences in the estimates are due to differences in predicted global BC concentrations, which are sensitive to emission and wet scavenging rates, to assumptions of the extent to which BC is mixed with other aerosols, to meteorological variables, such as surface albedo, and to vertical distribution of BC with respect to cloud layers. Even though the exact value of present day direct radiative forcing of BC is not known, all studies indicate a potential warming of the atmosphere caused by increased BC atmospheric loading since the preindustrial period.

[6] There are significant differences between the two radiatively active constituents of the atmosphere, GHGs and BC. As mentioned previously, the global distribution of CO_2 is relatively homogeneous such that globally averaged direct radiative forcing is a good measure of the climate response [*Hansen et al.*, 1984, 1997; *Forster et al.*, 2000; *Joshi et al.*, 2003]. Aerosols, however, are not homogeneously mixed in the atmosphere. BC, mainly anthropogenic in origin and with an atmospheric lifetime on the order of one week, is concentrated in continental regions where fossil fuel emissions and biomass burning are dominant. BC loading is also much higher in the Northern Hemisphere (NH) than in the Southern Hemisphere (SH). The inhomogeneity of the BC distribution means that, even if its globally averaged radiative forcing is relatively small, its regional impact can be significant. Annually averaged, the local column forcing for fossil fuel and biomass BC has been predicted to exceed 3.0 W m^{-2} at TOA in regions of high BC loading, such as Europe and eastern Asia [*Haywood and Ramaswamy*, 1998; *Koch*, 2001; *Chung and Seinfeld*, 2002]. On spatial scales smaller than the horizontal resolution of climate models, the forcing is even larger.

[7] In comparison to other aerosols, the magnitude of BC direct radiative forcing is similar to that of sulfate, for which the direct radiative forcing at TOA has been estimated to be in the range of -0.29 to -0.95 W m^{-2} [*Houghton et al.*, 2001]. However, BC aerosols differ profoundly from sulfates in their interaction with solar radiation in that sulfate aerosols radiatively cool both the surface and atmosphere by scattering solar radiation back to space, whereas BC radiatively warms the atmosphere by absorbing solar radiation but radiatively cools the surface by blocking solar radiation from reaching the surface. Negative forcing at the surface due to absorbing aerosols can be substantial and is supported by observational evidence [*Ramanathan et al.*, 2001b; *Markowicz et al.*, 2002]. The simultaneous surface cooling and warming at higher elevation have the potential to increase the static stability of the atmosphere. BC also differs from sulfate in that the contribution from cloudy regions to the total forcing for BC is higher than that of sulfate because a highly reflective cloud below a BC layer reflects more sunlight back to the BC layer, allowing BC to absorb even more radiation [*Haywood and Ramaswamy*, 1998].

[8] *Hansen et al.* [1997] and *Cook and Highwood* [2004] studied the climate sensitivity λ of absorbing aerosols by studying the change in λ as the single scattering albedo changes between 1.0 and 0.8, but with constant aerosol optical depth. Both studies concluded that absorbing aerosols do not follow the linear relationship in equation (1). In fact, the climate sensitivity λ may even be negative, depending on the single scattering albedo. The range of the values of single scattering albedo studied by *Hansen et al.* [1997] and *Cook and Highwood* [2004] is effectively for pure scattering aerosol or a mixture of scattering aerosol with a small component of an absorbing aerosol (e.g., BC). In comparison, the single scattering albedo of pure BC is only 0.4 (assuming optical properties from *d'Almeida et al.* [1991] and gamma size distribution with area-weighted effective radius of 0.1 μm and variance of 0.2). Therefore, the studies of *Hansen et al.* [1997] and *Cook and Highwood* [2004] do not applied directly to pure BC. Nevertheless, these studies suggest that, for BC, global and annual mean direct radiative forcing at TOA (or tropopause) may be an inadequate indicator of climate response.

[9] There have been numerous studies of the projected anthropogenic impact on climate change. Most studies consider only CO_2 and other GHGs while some also consider sulfate aerosol and ozone [see *Houghton et al.*, 2001, chapter 9]). Much less is understood about the climate impact of BC as there are relatively few studies on BC and climate. Recent global climate studies that have incorporated

BC include *Jacobson* [2002], *Menon et al.* [2002], *Wang* [2004], *Roberts and Jones* [2004], and *Jacobson* [2004].

[10] On the basis of six-year transient climate simulations with a mixed-layer ocean model, *Jacobson* [2002] predicts that removing fossil fuel emissions of BC and organic carbon (OC) would cool surface air by about 0.35 K after five years. The emission inventory used in that study is based on that of *Cooke et al.* [1999], giving 5.1 Tg yr^{-1} and 15.8 Tg yr^{-1} of fossil fuel BC and organic aerosol, respectively. The study of *Jacobson* [2002] is updated with the new emissions inventory of *Bond et al.* [2004] and to include the effect of BC absorption in snow and sea ice in *Jacobson* [2004]. The 10-year, globally averaged temperature response of fossil fuel and biofuel BC and OC is predicted to be about +0.27 K (+0.32 in the last 3 years). In both studies, aerosol optical properties were calculated assuming a shell and core model in which the core is comprised of BC and the shell consists of sulfate, nitrate, OC, sea salt, and mineral dust. Since fossil fuel BC and OC are considered together, the climate effects due to BC alone is not determined.

[11] *Menon et al.* [2002] use observed aerosol optical depth data in China, India, and the Indian Ocean to study the impact of increased BC in that region on global climate change. The effect of BC is determined from two 120-year climate simulations using observed sea surface temperature (SST). *Menon et al.* [2002] predict that BC over China, India, and the Indian Ocean cools surface temperature in China by 0.5 to 1 K but warms most of the world during June-July-August, especially in the Sahara Desert region and in west and central Canada. The study also predicts increased precipitation in southern China, India, and Myanmar and decreased precipitation to the south of those regions. Results of *Menon et al.* [2002] indicate that local tropospheric warming and dynamical export can lead to regional climate change away from the regions of radiative forcing.

[12] Another study on the climate impact of BC is *Wang* [2004]. In that study, the climate effect of 14 Tg yr^{-1} of BC is considered using different cases of SST. When SST is explicitly assigned based on observational data, BC is predicted to not cause a significant change in annually averaged global mean surface temperature. If a mixed-layer ocean model is used to calculate SST, *Wang* [2004] predicts that BC causes a slight warming of 0.09 K at the surface based on the average of the last twenty years of a sixty-year simulation. The results of *Wang* [2004] indicate that the impact of BC is more significant at the regional scale than at the global scale, such as the predicted change in precipitation patterns around the intertropical convergence zone (ITCZ). Because *Wang* [2004] considers BC to be externally mixed, its predicted 0.22 W m^{-2} BC forcing at TOA is on the lower end, and it is likely underestimated.

[13] To determine the climate sensitivity of direct radiative forcing of fossil fuel BC, *Roberts and Jones* [2004] use 4 times the fossil fuel emission rate of BC of *Cooke et al.* [1999] (20.2 Tg yr^{-1}). The rationale for quadrupling the emission rates is to increase signal-to-noise ratio of the climate model. Their results show that global and annual mean radiative forcing of fossil fuel BC scales linearly with emission rate; however, they do not show whether the climate sensitivity factor λ is constant for BC. From 30-year simulations using an atmosphere-ocean slab model, *Roberts and Jones* [2004] predict the climate sensitivity of direct radiative forcing of quadrupled fossil fuel BC to be 0.56 ± 0.06 K W^{-1} m^2, 40% less than that of CO_2 using the same climate model. Even though *Roberts and Jones* [2004] predict warming at the surface on the global scale, they also predict cooling over the surfaces of China, India, and parts of Africa, which they attribute to reduction of incident shortwave radiation by BC. Furthermore, similar to the results of *Wang* [2004], *Roberts and Jones* [2004] also predict a northward shift of the ITCZ.

[14] The purpose of this work is to study the climate response resulting from increased BC emissions since the preindustrial period. To allow for a more detailed examination of the climatic response due to absorbing aerosols, this study focuses on direct radiative forcing. Other effects, such as the first and second indirect forcing, are not considered. To address the uncertainty in the magnitude of predicted direct radiative forcing with respect to the mixing state of BC, two limiting cases are considered. In one case, BC is assumed to be physically separate from other particles, forming an external mixture. For the second case, BC is assumed to be homogeneously mixed with sulfate particles, forming an internal mixture. These two limiting cases provide upper and lower bounds for the radiative forcing of BC. Throughout, comparison with results of previous studies are made.

2. Model Description

[15] Global climate is simulated online in the Goddard Institute for Space Studies General Circulation Model II-prime (GISS GCM II') [*Hansen et al.*, 1983; *Rind and Lerner*, 1996]. To study the change in equilibrium climate due to direct radiative forcing of BC, results of three simulations are analyzed. In all three cases, monthly-mean, present-day (year 2000) concentrations of sulfate are used in the solar radiative flux calculations; also all three simulations predict BC concentrations online based on present-day emissions of BC. In the first simulation, which will be referred to as CONTROL, monthly mean concentrations of preindustrial BC and present-day sulfate are imported into the radiation scheme to calculate the baseline climate. Present-day sulfate and preindustrial BC are assumed to be externally mixed for this case. Also in the CONTROL simulation, anthropogenic direct radiative forcing of BC is calculated using online predicted present-day BC concentrations; however, the predicted anthropogenic BC forcing is not allowed to interact with the climate simulation, i.e., only preindustrial BC and present-day sulfate concentrations are incorporated into the radiative scheme for the climate simulation in CONTROL. In simulations EXTERNAL and INTERNAL, predicted present-day BC concentrations (instead of imported preindustrial BC concentrations) are allowed to interact with the climate simulation. In simulation EXTERNAL, BC is assumed to be externally mixed, whereas in simulation INTERNAL, BC is assumed to be internally mixed with present-level of sulfate aerosol. Note that the distinction between externally- and internally-mixed cases only refers to the optical properties of the assembly of BC and sulfate and not to

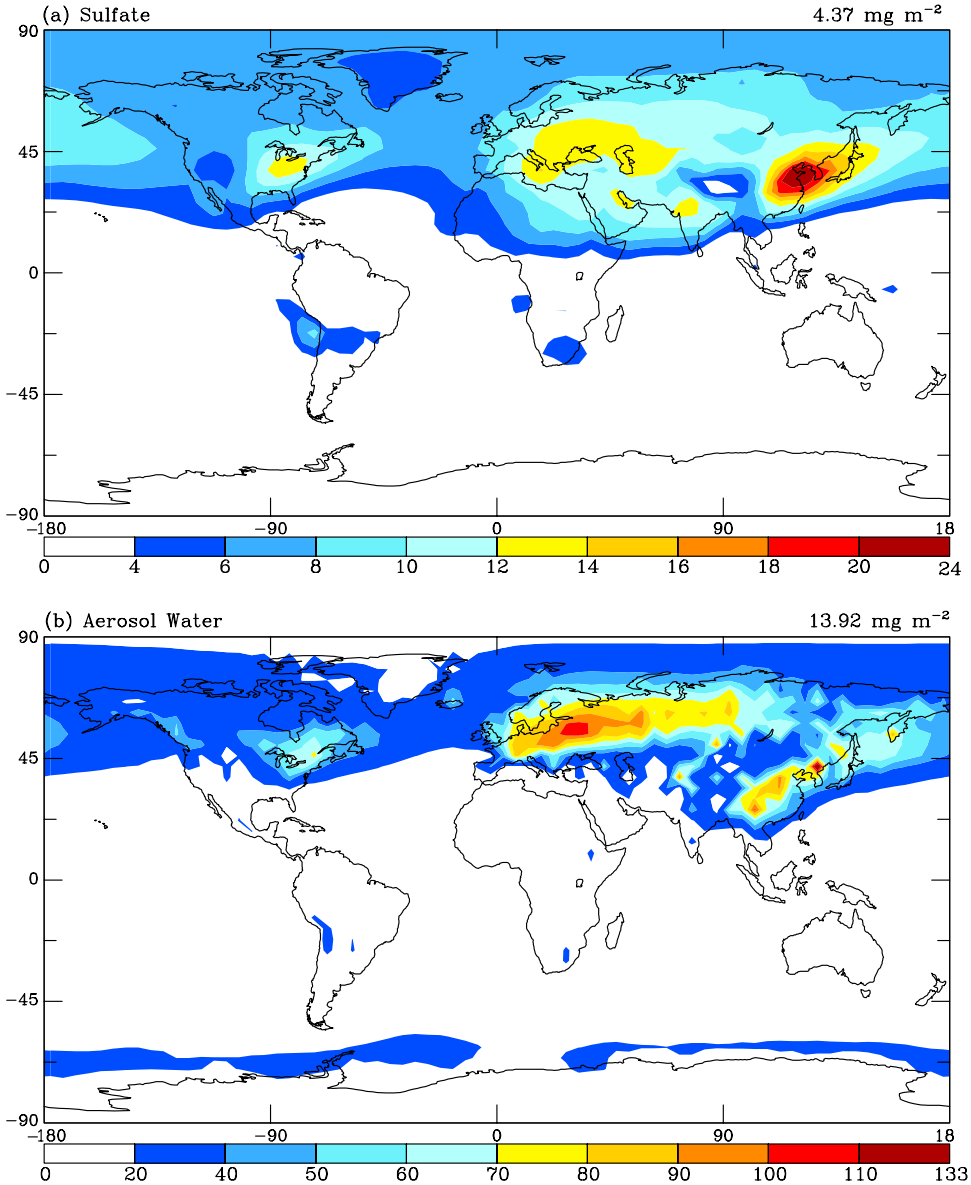

Figure 1. Present-day column burdens (mg m^{-2}) of (a) sulfate and (b) aerosol water used in this study. The global mean is provided on the upper right hand corner of each graph. The burdens are based on the averages of the last 3 years of a 61-month atmosphere-only GCM simulation.

the physical and chemical properties of the aerosols. The scavenging of BC particles (see section 2.3) is treated the same regardless of the mixing assumption. The differences in the predicted climate between CONTROL and that of EXTERNAL and INTERNAL are analyzed to determined the contribution of BC to climate change.

2.1. Climate Model: GISS GCM II-Prime

[16] The GISS GCM II' is summarized in *Hansen et al.* [1983] with updates in *Rind and Lerner* [1996], *Del Genio and Yao* [1993], and *Del Genio et al.* [1996]. The GCM has horizontal resolution of 4° latitude by 5° longitude and nine σ layers in the vertical, from the surface to 10 mbar. The vertical layers are centered at approximately 959, 894, 786, 634, 468, 321, 201, 103, and 27 mbar, with a 50-mbar surface layer.

[17] While prescribed seasonal ocean temperatures and ice cover are sufficient for studying the transport and distribution of BC, the climate, however, depends strongly on the underlying sea surface temperature (SST), which can change as BC alters the radiative balance of the climate system. Clearly, a reliable forecast of future climate depends upon the ability of the climate model to predict changes in ocean as well as atmosphere.

[18] To implement a model that allows realistic SST adjustment without using the computationally intensive coupled ocean-atmosphere model, climates are simulated in "Q-flux" mode, which uses a mixed-layer ocean model (also called slab ocean model) and is described in detail in *Hansen et al.* [1984] and *Russell et al.* [1984]. In this mode, the heat transport by the ocean current is held constant, but the ocean temperatures and ice cover are computed based on

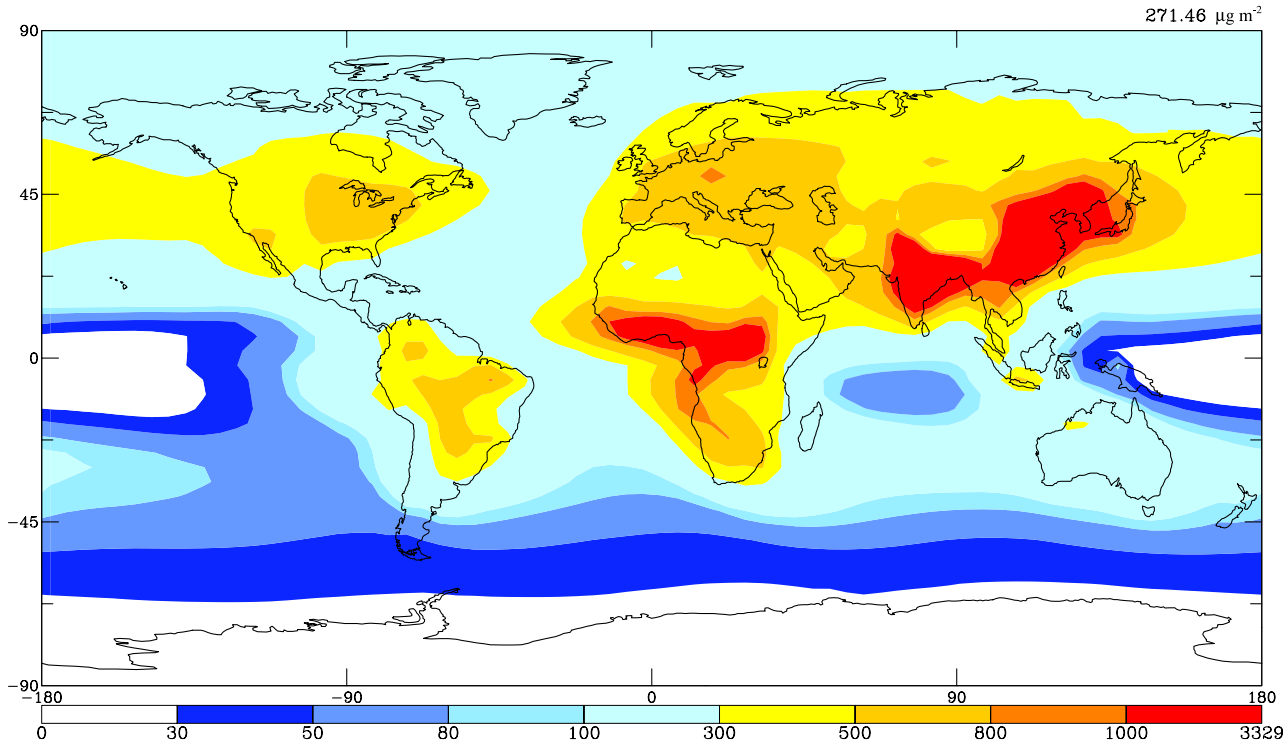

Figure 2. Estimated present-day BC column burden (μg m^{-2}). Results are averages of the last 75 years of simulation CONTROL.

energy exchange with the atmosphere, ocean heat transport, and the ocean mixed layer heat capacity. No exchange of heat between the mixed layer and the deeper ocean is assumed. Even though no feedback of climate change on ocean transport and heat exchange to the deeper ocean is allowed to occur, the atmospheric simulation is realistic and the results are a good approximation for modest climate perturbations. Ocean heat fluxes used in the current study are from the work of *Mickley et al.* [2004], which used the same version of the GCM as here. The climate sensitivity for this version of the GISS GCM is 4.2°C for doubled CO_2.

2.2. Background Sulfate Aerosol

[19] To study the effect of aerosol mixing state, global sulfate distributions are needed. Because the focus of this study is on black carbon, sulfate concentrations for all climate simulations are held constant at the present-day level. Monthly mean sulfate and associated aerosol water concentrations are calculated using the methodology of *Adams et al.* [2001]. The aerosol system of sulfate-ammonium-nitrate-water is simulated online in the GISS GCM with constant SST. The results of the last three years of simulation (after spin-up of 11 months) are averaged and used for subsequent climate simulations. For optical properties, all sulfate is assumed to be ammonium sulfate, but aerosol water content is determined from the the equilibrium water content of the bulk sulfate-ammonium-nitrate-water aerosol system, which is calculated based on the thermodynamic scheme ISORROPIA of *Nenes et al.* [1998]. Annually averaged, the predicted present-day sulfate and aerosol water global burdens are 2.2 Tg and 7.1 Tg, respectively. These values are slightly different from those of *Adams et al.* [2001] because here an updated gas-phase HNO_3 field from the Harvard-GISS GCM is used [*Mickley et al.*, 1999]. The current HNO_3 burden is lower, leading to lower aerosol nitrate, and therefore lower aerosol water content. Figure 1 shows the sulfate and aerosol water column burdens used in this study.

2.3. Simulation of Black Carbon

[20] Simulation of BC follows the methodology of *Chung and Seinfeld* [2002]. For the purpose of wet scavenging, BC is divided into hydrophobic and hydrophilic categories. Based on the estimates of *Cooke et al.* [1999], emitted BC is assumed to be 80% hydrophobic and 20% hydrophilic. Once emitted, ambient conversion of hydrophobic BC to hydrophilic BC occurs with an exponential decay lifetime of 1.15 days. Hydrophilic BC is assumed to be infinitely soluble in water whereas hydrophobic BC is assumed to be insoluble. Inside clouds, transport of dissolved hydrophilic BC follows the GCM treatment of liquid water [*Del Genio and Yao*, 1993; *Del Genio et al.*, 1996]. BC is either deposited (in case of precipitation) or returned to the air (in case of evaporation or detrainment). Below clouds, BC is scavenged according to a first-order parameterization that depends on the amount of precipitation [*Dana and Hales*, 1976; *Koch et al.*, 1999]. BC is also removed from the atmosphere by dry deposition with assumed dry deposition velocity of 0.1 cm s^{-1} [*Liousse et al.*, 1996].

[21] A major difference between the this study and that of *Chung and Seinfeld* [2002] in the simulation of BC is that the new emission inventory by *Bond et al.* [2004] is used here. In addition to considering fuel and economic sector as done in the earlier inventory by *Penner et al.* [1993], *Bond et al.* [2004] also take into account combustion type and

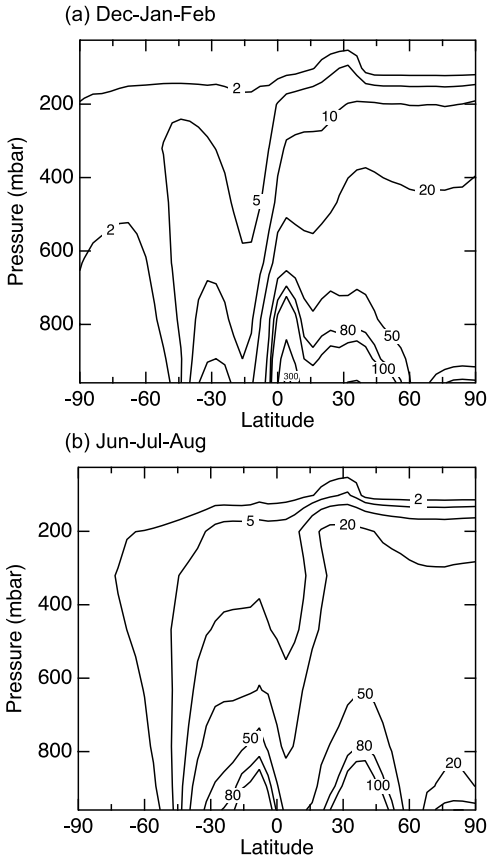

Figure 3. Estimated present-day zonal mean BC concentrations (ng m^{-3}) as a function of pressure for (a) December-January-February and (b) June-July-August. Results are averages of the last 75 years of simulation CONTROL.

emission controls. The current inventory is also an update in that it is based on fuel-usage data of 1996 instead of 1984. Estimated global BC emission rates are 1.6, 3.3, and 3.0 Tg yr^{-1} for biofuel, open burning, and fossil fuel, respectively. *Bond et al.* [2004] provide only annual emissions; the biomass burning inventory is distributed monthly by scaling the annual emissions by monthly fire counts of the Global Burned Area 2000 Project [*Grégoire et al.*, 2003]. Fossil fuel and biofuel emissions are assumed to be constant throughout the year.

[22] To estimate the monthly mean preindustrial concentrations of BC, the preindustrial biomass-burning emission level is assumed to be 10% of present-day and preindustrial fossil fuel emission is assumed to be zero. Preindustrial concentrations are simulated online in the GCM with constant SST. Results of the last three years of simulation after 11 months of spin up period are averaged and imported into the radiation code to calculate the baseline climate (simulation CONTROL). The estimated preindustrial global burden of BC is 0.01 Tg.

[23] The present-day BC concentrations are also simulated online in the simulation CONTROL. The predicted annual mean column burden of BC is shown in Figure 2. The predicted present-day BC burden is greatest in eastern United States, Europe, India, and China, where fossil fuel emissions are dominant, and in South America and southern Africa, where biomass emissions are high. The predicted present-day global BC burden is 0.14 Tg, which is lower than that of 0.22 Tg of *Chung and Seinfeld* [2002]; the explanation is the lower emission rates of the *Bond et al.* [2004] inventory versus that of *Penner et al.* [1993] inventory that was employed by *Chung and Seinfeld* [2002] (8 Tg yr^{-1} versus 12 Tg yr^{-1} globally). The largest differences occur in eastern Europe and northwestern United States, where the emission rate recommended by *Bond et al.* [2004] is about a factor of 5 lower and a factor of 3 higher than those of the previous emission inventory used, respectively.

[24] Predicted zonal mean BC concentrations as a function of pressure are shown in Figure 3. Except for the polar regions, predicted BC concentrations are the greatest at the surface and decrease as altitude increases, mostly due to removal by wet deposition. Elevated concentrations in the tropics reflect the significance of biomass burning. Transport from the midlatitudes to high latitudes leads to relatively high levels of BC above the surface in the polar regions.

2.4. Direct Radiative Forcing of Black Carbon

[25] Direct radiative forcing calculations of BC follows the method of *Chung and Seinfeld* [2002]. Optical properties (extinction efficiency, single-scattering albedo, and asymmetry parameter) of BC and sulfate aerosols are determined by Mie theory based on wavelength-dependent refractive indices and assumed size distributions. The particle size distribution is assumed to be the standard gamma distribution with area-weighted effective variance $v_e = 0.2$. The variance is assumed to be constant even when particles take up water and grow to larger sizes. For external mixture of BC and sulfate, the area-weighted effective radii for dry BC and sulfate are 0.1 μm and 0.3 μm [*Tegen et al.*, 2000] and particle densities are assumed to be 1.8 and 1.0 g cm^{-3} [*d'Almeida et al.*, 1991], respectively. Dry sulfate aerosol is represented as ammonium sulfate, with refractive indices from *Toon et al.* [1976]. The water uptake of ammonium sulfate aerosol is governed by thermodynamic equilibrium (see *Adams et al.* [1999] and section 2.2). Composite refractive indices of the aqueous sulfate aerosol are the volume-averaged refractive indices of ammonium sulfate and water. Refractive indices of water are taken from *d'Almeida et al.* [1991]. For BC refractive indices of soot in *d'Almeida et al.* [1991] are used. BC is assumed to not take up water. For an internal mixture of BC and sulfate aerosols, the area-weighted effective radius for the dry particle is assume to be 0.3 μm and particle density is the mass-averaged density of BC, $(NH_4)_2SO_4$, and water. The

Table 1. Summary of Direct Radiative Forcing Estimates of Anthropogenic BC[a]

	External			Internal		
	NH	SH	Global	NH	SH	Global
TOA	0.52	0.15	0.33	0.93	0.28	0.60
Atmosphere	1.33	0.43	0.89	1.92	0.62	1.27
Surface	−0.81	−0.28	−0.55	−1.00	−0.34	−0.67

[a]Units are in W m^{-2}.

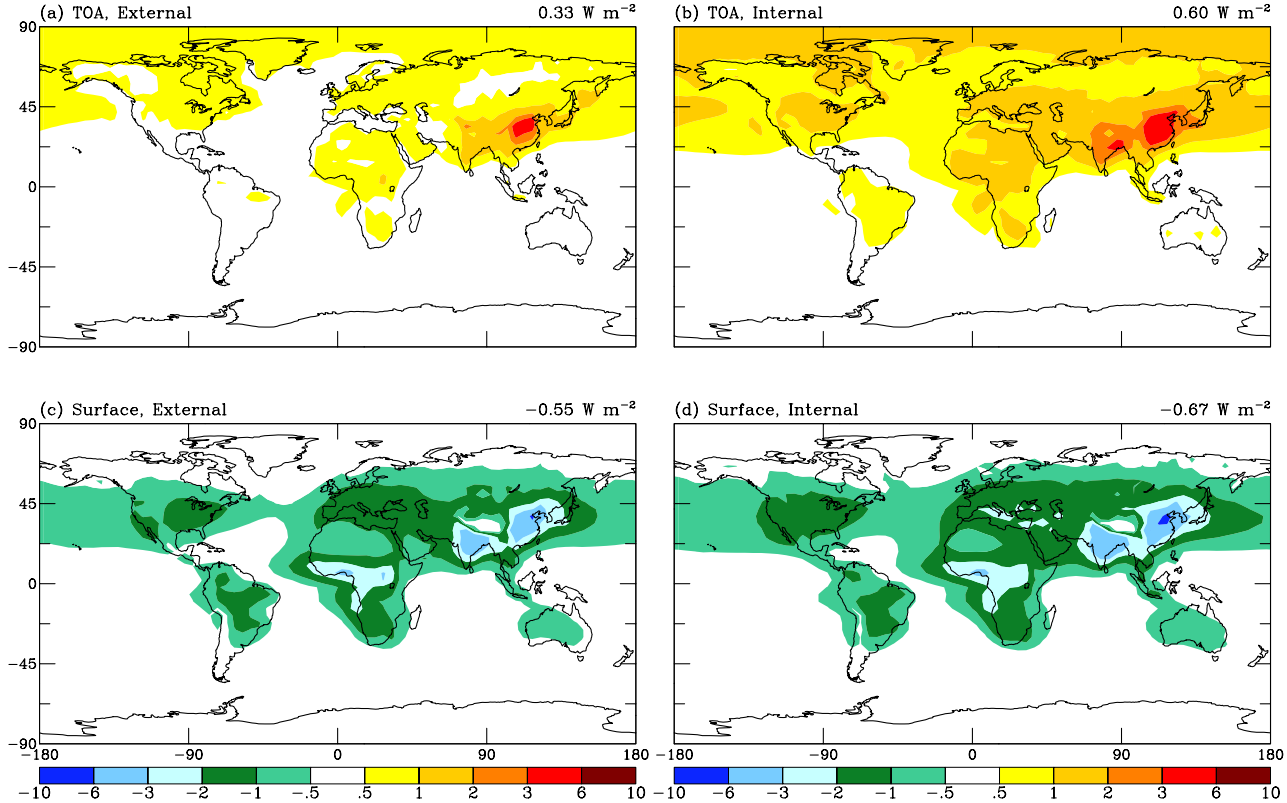

Figure 4. Geographical distributions of estimated anthropogenic contribution to annual mean direct radiative forcing (W m^{-2}) of BC at TOA (top panel) and the surface (bottom panel) for externally-mixed (left panel) and internally-mixed (right panel) BC. Results are averages of the last 75 years of simulation CONTROL.

refractive indices are calculated by volume-weighting the refractive indices of BC and $(NH_4)_2SO_4$, and water.

[26] Using the online concentrations of BC discussed in the previous section, direct radiative forcing of BC is calculated in simulation CONTROL. Direct radiative forcing is calculated at each model layer as the instantaneous difference in the solar radiative irradiance in the presence and absence of BC. At the surface, radiative forcing is calculated as the instantaneous difference in the absorbed solar radiation at the surface in the presence and absence of BC. During CONTROL simulation the radiation scheme is called three times during every radiation time step (5 hours). In the first two calls, imported present-day concentrations of aqueous sulfate aerosols and online concentrations of BC are used. In the first call, sulfate and BC are assumed to be externally mixed. For the second call, sulfate and BC are assumed to be internally mixed. The radiative fluxes during the first two calls are archived for diagnostics and do not affect the climate simulation. Finally, during the third call, the radiation scheme use the imported present-day sulfate and preindustrial BC concentrations. The difference in shortwave radiative fluxes between the first and third call is the direct radiative forcing of BC in an external mixture. Similarly, the difference in shortwave radiative fluxes between the second and third call is the direct radiative forcing of BC in an internal mixture. Note that present-day sulfate concentrations remain constant for all calls to the radiation scheme. The sulfate contribution to radiative forcing is assumed to stay constant whether sulfate and BC are externally or internally mixed; thus, the change in radiative irradiance between the externally- and internally-mixed cases is attributed to the enhancement of BC direct radiative forcing due to the change in mixing state. Direct longwave radiative forcing is neglected as it is expected to be small [*Haywood et al.*, 1997] (but the longwave climate response to BC shortwave direct radiative forcing is included). A summary of forcing estimates is given in Table 1.

2.4.1. Annual Mean Direct Radiative Forcing

[27] Anthropogenic BC is estimated to contribute to a globally and annually averaged direct radiative forcing of +0.33 W m^{-2} at TOA if considered to be externally mixed. The forcing efficiency of 2.4 W m^{-2} per Tg BC is similar to that of *Chung and Seinfeld* [2002] and *Koch* [2001], which also uses GISS GCM-II'. For comparison of forcing estimates with other models, see *Chung and Seinfeld* [2002]. If BC is assumed to be internally mixed with the present-day level of sulfate, the estimate increases to +0.60 W m^{-2}. The increase in warming is a result of the fact that the single scattering albedo of the assemblage of BC plus sulfate aerosol is lower under the internally mixed assumption. At the surface, anthropogenic BC direct radiative forcing is estimated to be −0.55 W m^{-2} and −0.67 W m^{-2} for the externally- and internally-mixed cases, respectively. The increase in surface cooling going from an external to an internal mixture of BC and sulfate is less than the corresponding increase in warming at

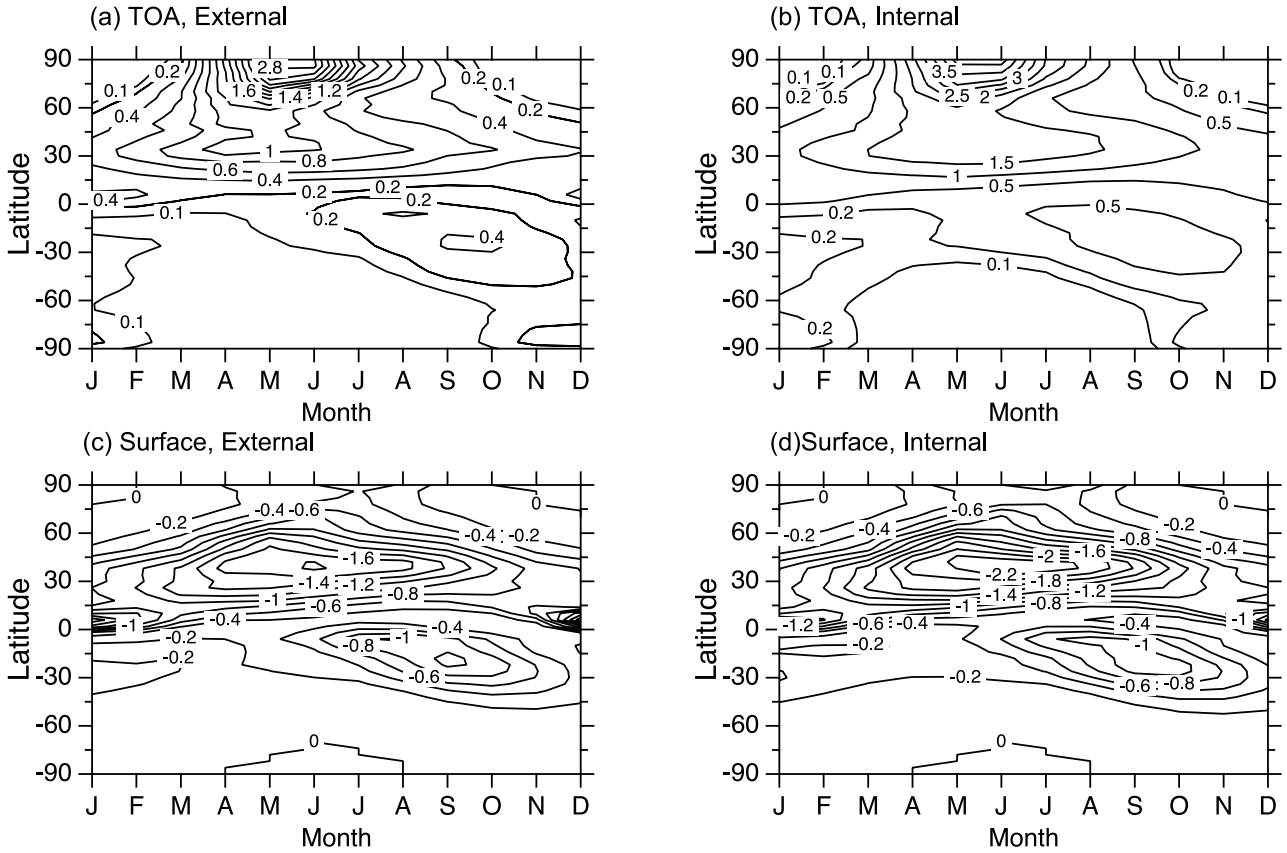

Figure 5. Estimated zonal and monthly mean anthropogenic contribution to direct radiative forcing (W m^{-2}) of BC at TOA (top panel) and the surface (bottom panel) for externally-mixed (left panel) and internally-mixed (right panel) BC. Results are averages of the last 75 years of simulation CONTROL.

TOA because the magnitude of the ratio of surface to TOA direct radiative forcing decreases with decreasing single scattering albedo (if surface and TOA forcing are of the opposite signs). Globally and annually averaged, the ratio of surface to TOA anthropogenic BC forcing decreases from 1.7 to 1.1 going from an external to an internal mixture of BC and sulfate. Subtracting surface forcing from TOA forcing, anthropogenic BC is predicted to warm the atmosphere by 0.89 W m^{-2} to 1.27 W m^{-2}.

[28] Figure 4 shows the geographical distribution of the estimated anthropogenic BC contribution to annual mean direct radiative forcing; the corresponding zonal and monthly mean is shown in Figure 5. The geographical distribution of direct radiative forcing at TOA is determined by two factors: the column burden of BC and the reflectivity of the surface underneath the BC layer. These two factors cause TOA forcing to be the largest in eastern China, where the annually averaged forcing is estimated to be 5–6 W m^{-2}. Not only is the BC loading high in eastern China (see Figure 2), the underlying desert surface is highly reflective. In contrast to the midlatitudes, BC loading in the northern high latitudes is relatively small; however, due to the high surface albedo from snow and ice, direct radiative forcing in the northern high latitudes is still high. As seen from Figures 4a and 4b, TOA forcing increases everywhere if BC is assumed to be internally mixed with sulfate, as most areas of high BC loading overlap with areas of high aerosol sulfate loading. In contrast to forcing at TOA, the forcing at the surface is concentrated in the midlatitudes where BC loading is the greatest (Figures 4c and 4d). Because surface forcing decreases as surface albedo increases, surface forcing in the northern high latitudes is actually very low even though the TOA forcing is high. As mentioned earlier, the increase in surface cooling from the internal to external mixture assumption is less than the increase in warming at TOA. Overall, both TOA and surface direct radiative forcings are concentrated in the NH.

2.4.2. Seasonal and Zonal Mean Direct Radiative Forcing

[29] The zonal and monthly means of estimated BC direct radiative forcings at TOA and the surface are shown in Figure 5. Between 30°N and 90°N, TOA and surface forcings peak from April to June, which is the period of maximum BC emission in the NH from biomass burning. During this period of high BC emission in the NH, TOA forcing is the largest in the northern polar region because both surface albedo and solar insolation are high. Surface forcing, on the other hand, peaks at 35°N, where zonal mean emissions are largest. During the northern winter months, direct radiative forcing remains high at midlatitudes because of fossil fuel emissions. In comparison to the NH, peak forcing in the SH is an order of magnitude lower at TOA and a factor of two lower at the surface. The seasonal pattern of forcing in the SH also follows the seasonal cycle of biomass emission, which is largest from August to October in the SH. Zonally, maximum forcing occurs

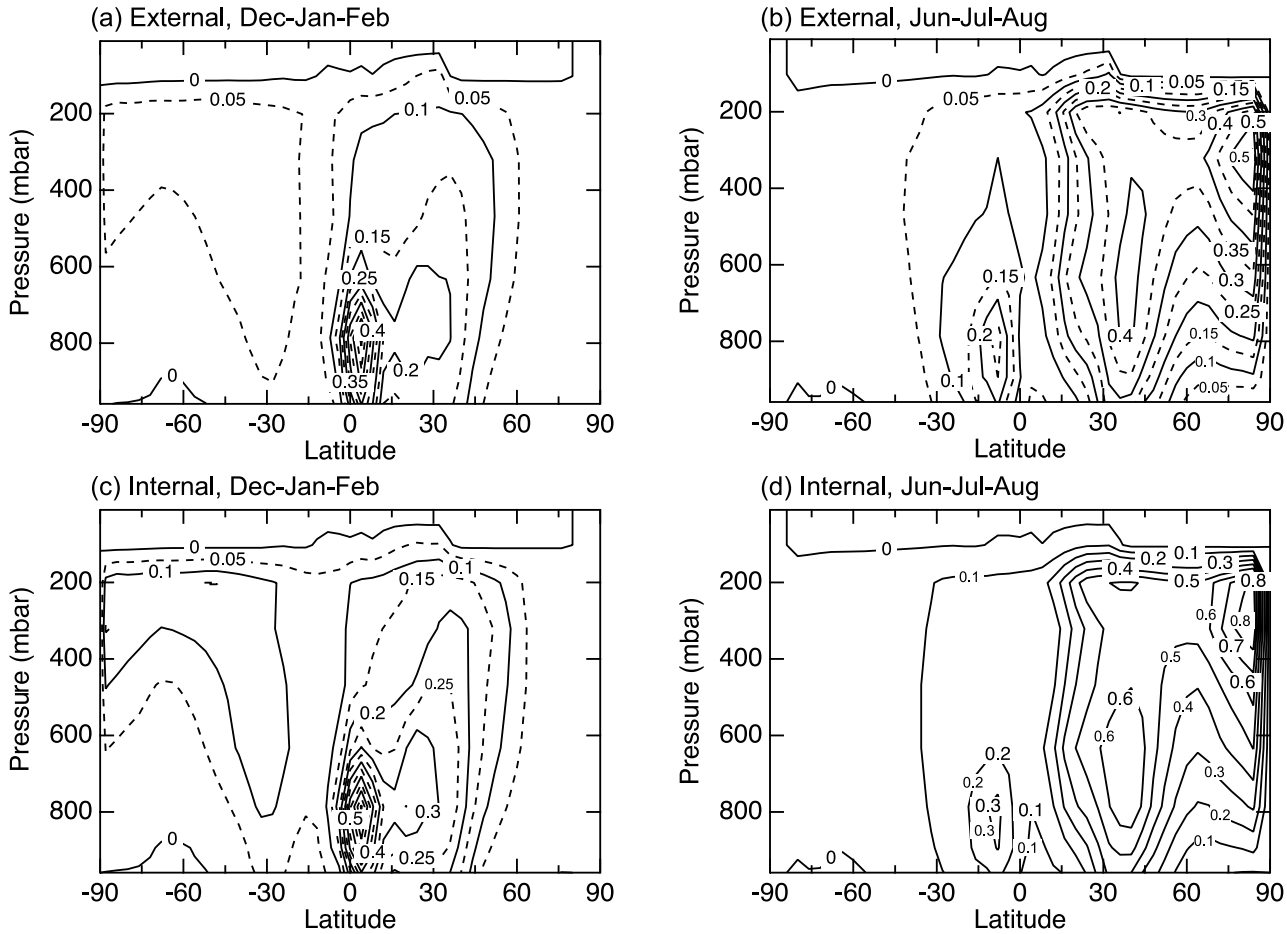

Figure 6. Estimated zonal mean anthropogenic contribution to direct radiative forcing (W m^{-2}) of BC as a function of pressure for December-January-February (left panel) and June-July-August (right panel) for externally-mixed (top panel) and internally-mixed (bottom panel) BC. Except for Figure 6d, contour lines are in 0.05 W m^{-2} increments. Results are averages of years 26 to 30 of simulation CONTROL.

around 20°S, overlapping with the region of highest emissions. With essentially no emissions south of 40°S, BC concentrations are so low that direct radiative forcing is extremely low in the southern polar regions. When BC is assumed to be internally mixed with the present-day level of sulfate, the seasonal and zonal patterns of anthropogenic BC radiative forcing remain the same; only the magnitude of the forcing is higher.

[30] Figure 6 shows the predicted zonal mean BC direct radiative forcing as a function of pressure for both externally- and internally-mixed BC. The contrast between the northern winter (December-January-February or DJF) and summer (June-July-August or JJA) months is clearly evident. During the northern winter, direct radiative forcing is concentrated near the tropics, where BC concentrations are high. Unlike the distribution of BC concentration, however, forcing is not largest near the surface, but around 800 mbar. The reason for this is that BC above cloud layers results in higher forcing due to the high cloud reflectivity. As mentioned earlier, the largest forcing occurs during the NH summer months at northern high latitudes. Figure 6 indicates that maximum forcing in JJA occurs at around 300 mbar (approximately 9 km in elevation). Again, even though BC concentra-

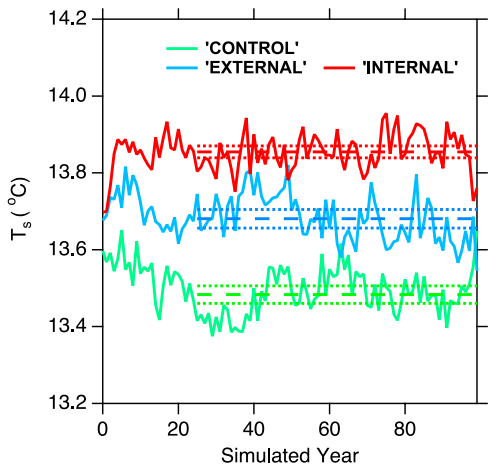

Figure 7. Modeled global and annual mean surface air temperature versus simulation year. The dashed lines are means of the last 75 years of simulation; the dotted lines indicate 95% confidence intervals of the means.

Table 2. Summary of Annual Mean Differences and 95% Confidence Intervals of Selected Climate Variables

	EXTERNAL-CONTROL			INTERNAL-CONTROL			INTERNAL-EXTERNAL		
	NH	SH	Global	NH	SH	Global	NH	SH	Global
Surface Air Temperature, K	0.29 ± 0.05	0.11 ± 0.03	0.20 ± 0.03	0.54 ± 0.04	0.20 ± 0.03	0.37 ± 0.03	0.25 ± 0.04	0.10 ± 0.03	0.17 ± 0.03
Land Temperature, K	0.31 ± 0.06	0.14 ± 0.05	0.26 ± 0.04	0.59 ± 0.05	0.30 ± 0.05	0.50 ± 0.04	0.28 ± 0.05	0.16 ± 0.06	0.24 ± 0.03
Sea Surface Temperature, K	0.19 ± 0.15	0.07 ± 0.22	0.12 ± 0.28	0.36 ± 0.12	0.13 ± 0.12	0.23 ± 0.12	0.17 ± 0.15	0.06 ± 0.17	0.11 ± 0.23
Precipitation, mm day^{-1}	0.030 ± 0.010	−0.023 ± 0.010	0.003 ± 0.003	0.057 ± 0.009	−0.035 ± 0.009	0.011 ± 0.003	0.027 ± 0.009	−0.012 ± 0.009	0.008 ± 0.003
Total Cloud Cover, %	0.28 ± 0.16	−0.14 ± 0.09	0.07 ± 0.08	0.44 ± 0.15	−0.22 ± 0.09	0.11 ± 0.08	0.16 ± 0.13	−0.08 ± 0.09	0.04 ± 0.07
Cloud Top Pressure, mbar	−0.7 ± 0.8	2.1 ± 0.7	0.7 ± 0.4	−2.0 ± 0.8	2.7 ± 0.6	0.3 ± 0.4	−1.3 ± 0.7	0.6 ± 0.7	−0.4 ± 0.4
Precipitable Water, mm	0.56 ± 0.08	0.20 ± 0.07	0.38 ± 0.07	1.03 ± 0.07	0.38 ± 0.07	0.70 ± 0.06	0.47 ± 0.08	0.18 ± 0.08	0.32 ± 0.08
Surface Albedo, %	−0.15 ± 0.05	−0.00 ± 0.01	−0.08 ± 0.03	−0.29 ± 0.05	−0.01 ± 0.01	−0.15 ± 0.03	−0.14 ± 0.05	−0.01 ± 0.01	−0.07 ± 0.03
Net SW at TOA, W m^{-2}	0.45 ± 0.10	0.21 ± 0.08	0.33 ± 0.06	0.82 ± 0.10	0.35 ± 0.08	0.58 ± 0.06	0.36 ± 0.10	0.14 ± 0.08	0.25 ± 0.06
Net LW at TOA, W m^{-2}	−0.27 ± 0.12	−0.48 ± 0.10	−0.37 ± 0.05	−0.49 ± 0.12	−0.77 ± 0.08	−0.63 ± 0.05	−0.22 ± 0.11	−0.29 ± 0.08	−0.26 ± 0.05
Net SW at Surface, W m^{-2}	−1.03 ± 0.10	−0.32 ± 0.08	−0.68 ± 0.06	−1.35 ± 0.11	−0.42 ± 0.08	−0.89 ± 0.07	−0.32 ± 0.11	−0.10 ± 0.08	−0.21 ± 0.07
Net LW at Surface, W m^{-2}	0.56 ± 0.11	0.28 ± 0.06	0.42 ± 0.07	0.95 ± 0.11	0.44 ± 0.07	0.69 ± 0.07	0.39 ± 0.10	0.16 ± 0.06	0.27 ± 0.07
Latent Heat Flux, W m^{-2}	0.02 ± 0.14	−0.21 ± 0.10	−0.09 ± 0.09	−0.28 ± 0.12	−0.35 ± 0.11	−0.31 ± 0.09	−0.30 ± 0.15	−0.14 ± 0.11	−0.22 ± 0.09
Sensible Heat Flux, W m^{-2}	0.45 ± 0.06	0.19 ± 0.04	0.32 ± 0.04	0.71 ± 0.07	0.25 ± 0.04	0.48 ± 0.04	0.25 ± 0.06	0.06 ± 0.04	0.15 ± 0.03

tions here are not very high (about 20 ng m^{-3}), the high reflectivity of the underlying ice and snow surfaces causes direct radiative forcing to be large.

3. Results and Discussion

[31] All three climate simulations (CONTROL, EXTERNAL, and INTERNAL) have been carried out for 100 years. The first 25 years are used as spin-up to allow the model sufficient time to reach equilibrium. Results presented in this section are averaged over the last 75 years of each simulation. Assuming that results of each year represent one set of data, statistical analysis based on the two-sample "usual" t-test of *Zwiers and von Storch* [1995] is applied to the results of the last 75 years of each simulation. For latitude-longitude plots, the mean and other statistics are calculated at each grid box without taking into account of spatial correlation. For pressures-zonal plots, statistical analysis are applied after zonal and pressure means have been calculated. Note that the "usual" t-test of *Zwiers and von Storch* [1995] differs from that of the traditional Student's t-test in that the "usual" t-test does not assume that the results of each simulation year to be independent. For this study in which $n = 75$ for using results from the last 75 years of each simulation, if Student's t-test is applied directly, the difference in means is considered to be significant at 95% confidence level if the difference is greater than $1.98 \times s\sqrt{2/n}$, where s is the standard deviation of the climate variable of interest. However, Student's t-test assumes that the number of samples to be independent. Since in this study the results from the 75 sampled years are from the same simulation, the independence assumption is not valid. In the "usual" t-test, the difference in means is significant at the 95% confidence interval if it is greater than $1.98 \times s\sqrt{1/\hat{n}_e + 1/\hat{m}_e}$, where $\hat{n}_e < n$ and $\hat{m}_e < n$ are the equivalent sample sizes for the two simulations to be compared. In the case that $\hat{n}_e + \hat{m}_e < 30$, a lookup table is utilized. For details on how to calculate equivalent sample size and more rigorous explanation of the "usual" t-test, please refer to *Zwiers and von Storch* [1995]. For the three simulations carried out in this study, $\hat{n}_e$ and $\hat{m}_e$ are on the order of 30, but vary depending on the climate variable and location of interest.

[32] Unless otherwise specified, all results shown are significant at the 95% level. Also note that the statistical analysis is applied only to the variability of the model output; uncertainties of model parameterization, emission rates, subgrid variabilities, etc. are not considered. Figure 7 shows the surface air temperature for all three 100-year simulations. The figure indicates that each simulation has equilibrated at a different climate state. A summary of estimated annual mean change of selected climate variables is given in Table 2.

3.1. Annual Mean Surface Air Temperature Response

[33] The geographical distribution of the equilibrium annual mean surface air temperature response attributed to direct radiative forcing of anthropogenic BC is shown in Figure 8. Even though the forcing resulting from BC at the surface is negative, BC forcing is positive in the air immediately above the surface, and the surface air temperature is predicted to increase. Globally and annually aver-

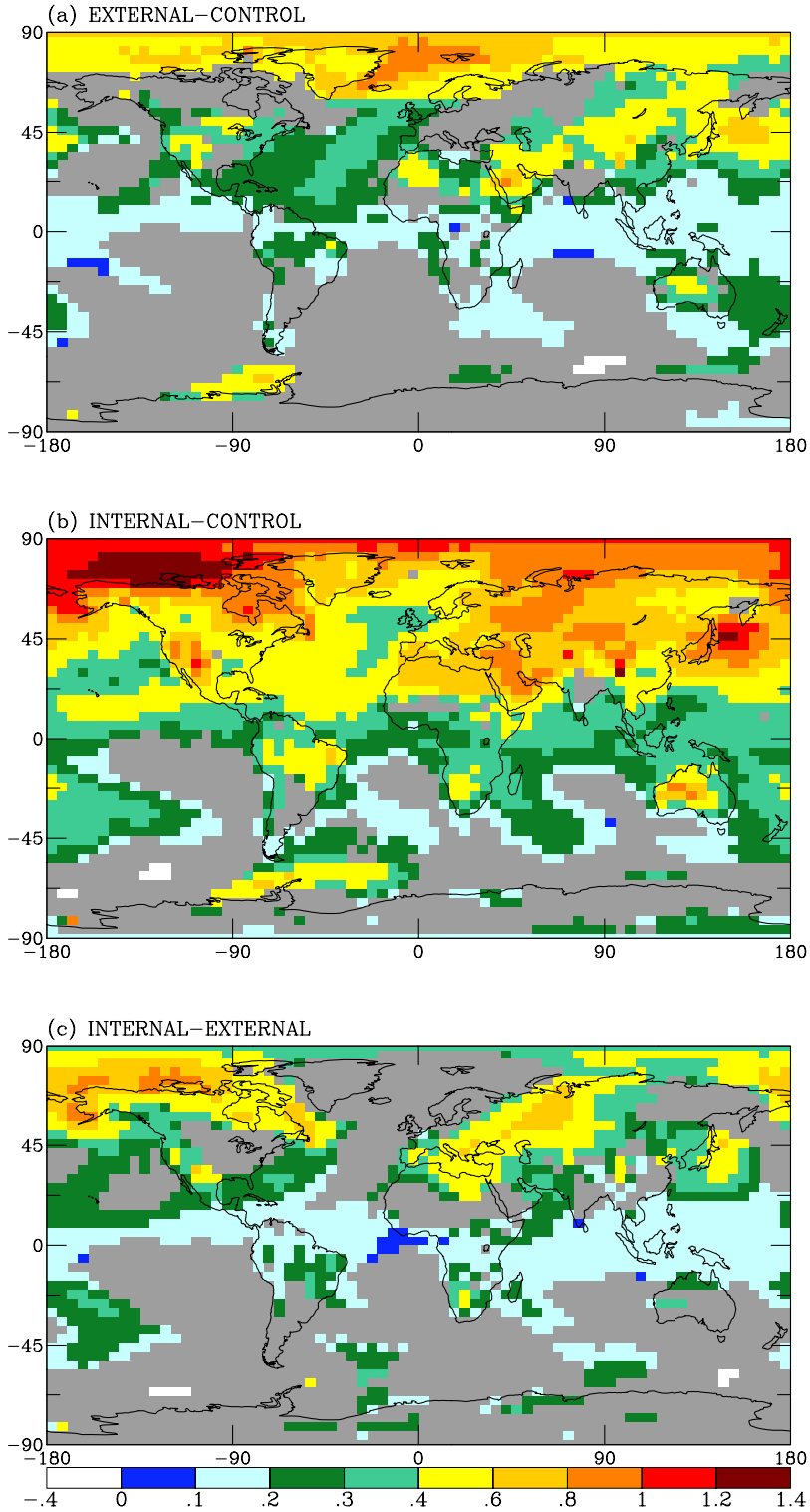

Figure 8. Estimated change in equilibrium annual mean surface air temperature (K) for (a) EXTERNAL minus CONTROL, (b) INTERNAL minus CONTROL, and (c) INTERNAL minus EXTERNAL. Gray indicates areas where the change is not significant at the 95% confidence level.

aged, the surface air temperature is predicted to rise by 0.20 and 0.37 K for the externally- and internally-mixed cases, respectively. Clearly, uncertainty in direct radiative forcing due to the mixing state leads to significant difference in the temperature response.

[34] In both the externally- and internally-mixed cases, the temperature response is concentrated more in the NH, which is expected since radiative forcing is strongest in the NH. The estimated surface temperature increase is 0.29 to 0.54 K for the NH and 0.11 to 0.20 K for the SH. Other than

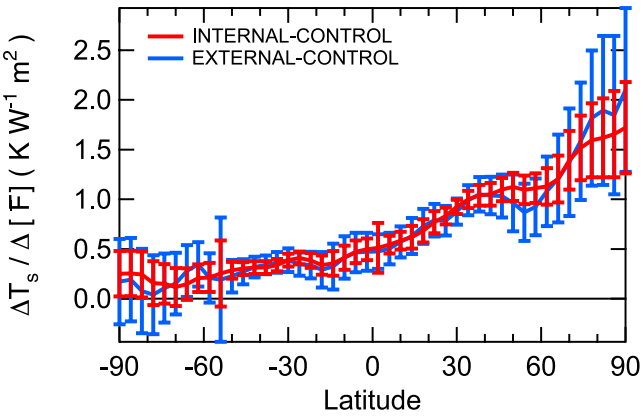

Figure 9. Estimated change in zonal and annual mean surface air temperature normalized by global and annual mean instantaneous direct radiative forcing at TOA. The error bars indicate 95% confidence intervals assuming zero uncertainty for the direct radiative forcing estimates.

the hemispheric pattern, however, the geographical pattern of the surface temperature response does not follow that of the direct radiative forcing and the maximum response does not occur over regions of largest forcing. Previous studies have shown that temperature response to radiative forcing is largest in the high latitudes independent of the type of forcing (i.e., solar, CO_2, ozone, or cloud forcing), e.g., *Manabe and Wetherald* [1975], *Chen and Ramaswamy* [1996a], *Hansen et al.* [1997], *Forster et al.* [2000], *Boer and Yu* [2003], *Joshi et al.* [2003], and *Mickley et al.* [2004]. The predictions here for BC direct radiative forcing exhibit a similar pattern, with the temperature response in high northern latitudes being as large as 1.4 K in annual mean. Figure 9 shows the zonal mean change in annual mean temperature weighted by the globally and annually averaged forcing at TOA. Figure 9 indicates that the zonal mean surface temperature response is very similar for externally- and internally-mixed BC and that the response is clearly maximum in the northern high latitudes. Note that zonally and annually averaged, the largest forcing occurs at around 30°N and in the northern polar region and is about 0.8 W m^{-2} and 1.4 W m^{-2} for externally- and internally-mixed BC, respectively.

[35] Other than the northern high latitudes, when BC is externally mixed, substantial surface warming is predicted over most of Asia, as well as remote regions of the Atlantic and the Pacific, even extending to parts of the SH. The temperature response over the high BC emission regions of Europe and North America is actually insignificant in comparison to the model variability. If BC is assumed to be internally mixed with sulfate, however, then substantial surface warming is predicted to occur throughout the entire NH as well as a significant portion of the SH, including parts of South America and most of southern Africa, Australia, and southern Pacific. Notice that even though the absolute temperature increase in the tropics is relatively small in comparison to that of the high northern latitudes, relative to the natural variability (as measured by the standard deviation of model output) of the respective latitude, the temperature increase in the tropics is much higher. Figure 10 shows the estimated ratio of the change to the standard deviation of annual mean surface air temperature. Over the tropics, the predicted change in surface air temperature is on the order of one standard deviation for externally-mixed BC. For internally-mixed BC, the temperature increase is on the order of three standard deviations. As *Menon et al.* [2002] and *Roberts and Jones* [2004] have already suggested, Figures 8 and 10 strongly indicate that the effect of BC radiative forcing is not local, but in fact can alter the climate of remote regions.

[36] Even though the climate sensitivity of BC predicted here is similar to the prediction of *Roberts and Jones* [2004] (see section 3.2), the results here differ in one significant way: *Roberts and Jones* [2004] predict small cooling of surface air in some regions, such as in China and India, whereas in this study no significant surface cooling is predicted anywhere. As mentioned previously, absorption of BC in the atmosphere reduces incident solar radiation at the surface, potentially leading to cooling at the surface. If results from years 20 to 30 of each simulation of this study were analyzed (to parallel *Roberts and Jones* [2004] study), surface cooling would have been predicted in some regions, but the cooling is statistically insignificant. Thereafter the climate equilibrates and the reduction in solar radiation at the surface is compensated by the changes in longwave radiative flux, sensible heat flux, and latent heat flux (see section 3.6 later); eventually warming or no change is predicted everywhere at the surface. Lacking statistical information, and given the relatively short simulations of *Roberts and Jones* [2004], detailed comparison between this study and *Roberts and Jones* [2004] is difficult.

[37] In comparison to the surface air temperature response induced by ozone and equivalent CO_2 forcings studied by *Mickley et al.* [2004], there are both similarities and differences. Direct comparison of this study and *Mickley et al.* [2004] is particularly useful because both studies use the same climate model. *Mickley et al.* [2004] examine the climate response of direct radiative forcing of anthropogenic ozone and a 25-ppm increase in CO_2 concentration from the present-day level. In both cases, the annually and globally averaged instantaneous radiative forcing at the tropopause is estimated to be 0.49 W m^{-2}, which lies between that of 0.33 and 0.60 W m^{-2} for BC estimated here. Note that *Mickley et al.* [2004] report only the instantaneous forcing at the tropopause. As mentioned in section 1, adjusted forcing is a better of measure of potential climate response than instantaneous forcing. Unlike BC, for which instantaneous forcing at TOA, instantaneous forcing at tropopause, and adjusted forcing at tropopause are all approximately equal, adjusted forcings at the tropopause are typically 10–20% less than the instantaneous forcings at the tropopause for CO_2 and ozone [*Hansen et al.*, 1997; *Mickley et al.*, 2004]. The estimated climate sensitivity of 0.6 K W^{-1} m^{-2} for BC calculated here is within 15% of the climate sensitivity of ozone and about 30% less than that of CO_2, as calculated by *Mickley et al.* [2004] but taking into the account of the 10–20% reduction for the forcings of ozone and CO_2. The difference in climate sensitivities of BC and ozone is within the uncertainties of the model, despite the fact that the geographical and seasonal patterns of ozone radiative forcing are different from those of BC. The 30% reduction in the climate sensitivity of BC compared to that of CO_2 is

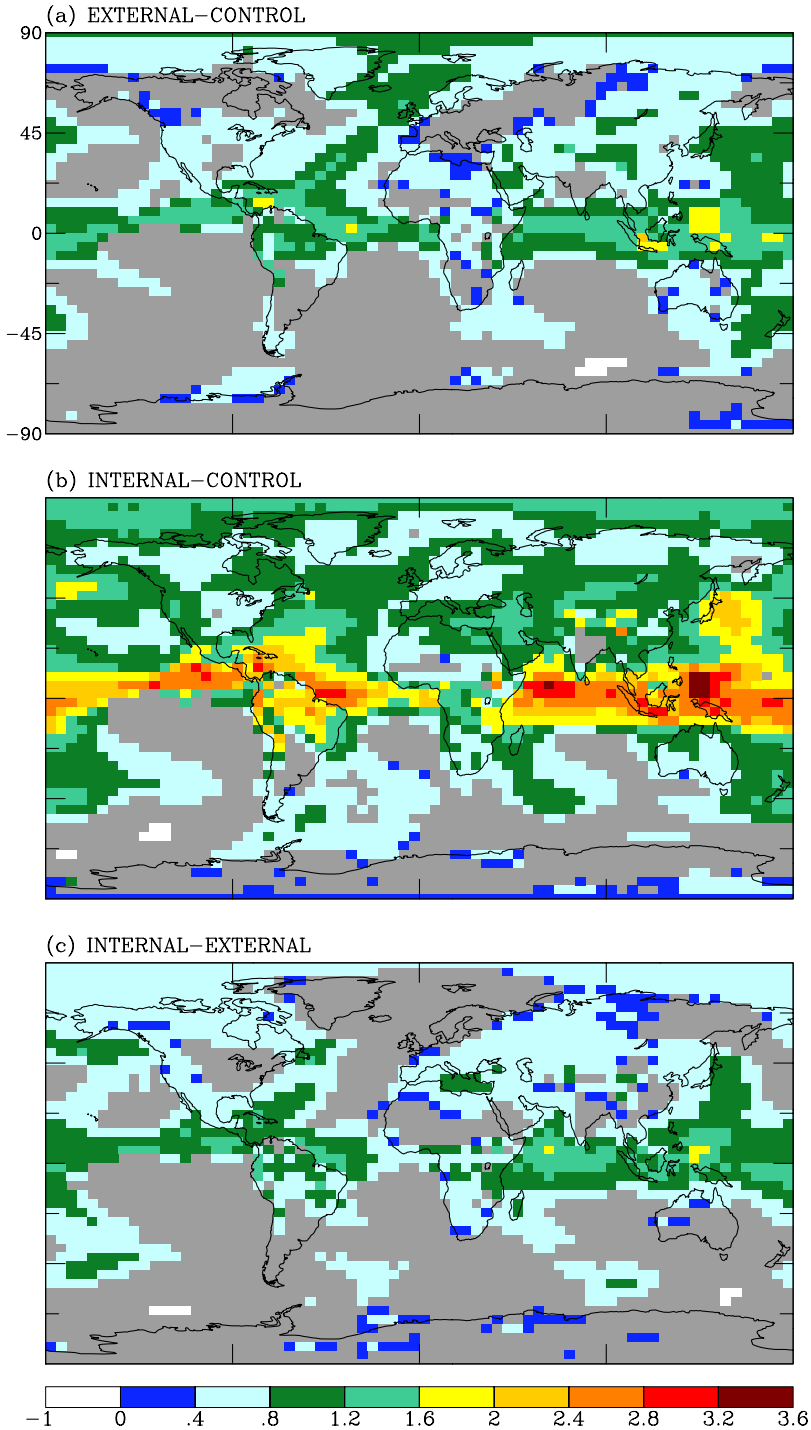

Figure 10. Grid by grid estimated ratio of equilibrium change to standard deviation of annual mean surface air temperature for (a) EXTERNAL minus CONTROL, (b) INTERNAL minus CONTROL, and (c) INTERNAL minus EXTERNAL. Gray indicates areas where the change is not significant at the 95% confidence level.

similar to the 40% reduction found by *Roberts and Jones* [2004]. The reason for the lowered climate sensitivity of BC in comparison to that CO_2 found in this study and in *Roberts and Jones* [2004] is not known.

[38] In all three cases, the maximum temperature increase is still in the northern high latitudes, indicating that, to some extent, regional differences in forcing are diluted in the temperature response. However, regional differences do exist. For example, annual mean surface air temperature is estimated to increase by about 0.6 to 0.8 K in central and eastern Russia, where no significant increase is predicted for ozone or CO_2 forcing. The reason for the difference is likely because radiative forcing over China is larger for BC than for CO_2 and ozone (estimated annual mean direct

Table 3. Climate Sensitivity of Absorbing Aerosol From Previous Studies[a]

Reported in Literature				Equations (5)–(9) Using $\omega_{abs} = 0.38$		
ω	$\Delta[\bar{F}]$, W m^{-2}	$\Delta[\bar{T}_s]$, K	λ, K W^{-1} m^2	τ_{sca}	$\Delta[\bar{F}_{abs}]$, W m^{-2}	λ_{abs}, K W^{-1} m^2
Hansen et al. [1997]						
1	−2.43	−2.12	0.87	0.1	0	...
0.95	−1.61	−0.94	0.58	0.092	0.62	1.62
0.90	−0.82	0.17	−0.21	0.084	1.22	1.60
0.85	−0.03	1.01	−33.70	0.076	1.81	1.44
0.80	0.74	1.90	2.57	0.068	2.39	1.40
Cook and Highwood [2004]*; Lower Troposphere*						
1	−4.72	−1.70	0.36	0.2	0	...
0.95	−3.02	−0.60	0.20	0.18	1.32	0.73
0.90	−1.40	0.60	−0.43	0.17	2.56	0.79
0.85	0.14	1.80	12.86	0.15	3.72	0.83
0.80	1.61	2.90	1.80	0.14	4.81	0.84
Cook and Highwood [2004]*; Midtroposphere*						
1	−4.90	−1.80	0.37	0.2	0	...
0.95	−2.28	−0.90	0.39	0.18	2.22	0.34
0.90	0.23	−0.10	−0.43	0.17	4.34	0.32
0.85	2.64	0.60	0.23	0.15	6.35	0.31
0.80	4.95	1.20	0.24	0.14	8.27	0.29

[a]Note the climate sensitivity for double CO_2 is 0.92 and 0.47 K W^{-1} m^2 for the climate models used in *Hansen et al.* [1997] and *Cook and Highwood* [2004], respectively.

radiative forcings over China are approximately 5 W m^{-2}, 0.5 W m^{-2}, and 0.1 W m^{-2} for anthropogenic BC, anthropogenic ozone, and 25-ppm increase in CO_2, respectively). Similarly for western Europe, significant warming is predicted only for BC, though only if BC were internally-mixed with sulfate. Here, predicted forcing for BC mixed internally with sulfate is slightly higher than that of O_3 and CO_2. The warming in eastern China and western Europe may also be caused by nonlocal radiative forcing. For example, *Menon et al.* [2002] predict BC in Asia causes warming over most of Europe even with fixed SST.

3.2. Climate Sensitivity of Black Carbon

[39] For both externally- and internally-mixed BC the climate sensitivity of direct radiative forcing of anthropogenic BC predicted here is ~0.6 K W^{-1} m^2, which is very similar to that predicted by *Roberts and Jones* [2004] for quadrupled fossil fuel BC (0.56 K W^{-1} m^2 with 95% confidence interval of ±0.06). Note that the climate sensitivity for double CO_2 of the Hadley Centre climate model used in *Roberts and Jones* [2004] is 0.9 K W^{-1} m^2, comparable to 0.8 K W^{-1} m^2 for the climate model used in this study. The fact that climate sensitivity is independent of the mixing assumption suggests that the linear relationship of equation (1) is still valid for BC, contrary to the conclusion of *Hansen et al.* [1997] and *Cook and Highwood* [2004]. The difference can be explained by the fact that the climate sensitivities reported in *Hansen et al.* [1997] and *Cook and Highwood* [2004] are for a mixture of purely scattering aerosol with small amount of absorbing material. Relevant results from *Hansen et al.* [1997] and *Cook and Highwood* [2004] are reproduced in Table 3. Based on the λ calculated for aerosols with single scattering albedo ω between 0.8 and 1.0 and at fixed optical depth, both studies conclude that the proportionality between $\Delta[\bar{T}_s]$ and $\Delta[\bar{F}]$ is not constant (see column 4 of Table 3). The climate sensitivity factor λ calculated by *Hansen et al.* [1997] and *Cook and Highwood* [2004], however, is not only for absorbing aerosols. The climate sensitivity of absorbing aerosols can be inferred from the results of *Hansen et al.* [1997] and *Cook and Highwood* [2004] by the following method.

[40] Assuming that the linear relationship of equation (1) holds for purely scattering aerosols, then the contribution of surface air temperature change from a purely scattering aerosol is given by

$$\left[\Delta\bar{T}_{s,sca}\right] = \lambda_{sca}\Delta[\bar{F}_{sca}] \tag{2}$$

In the case studied by *Hansen et al.* [1997], for example, λ_{sca} = 0.87 K W^{-1} m^2 (fifth row and fourth column of Table 3). *Hansen et al.* [1997] and *Cook and Highwood* [2004] study the effect of absorbing aerosols by reducing the single scattering albedo ω but keeping the optical depth τ_{total} constant. Reducing the single-scattering albedo from unity is equivalent to physically removing a small portion of the purely scattering aerosol and replacing it with an absorbing aerosol. Under the external mixture assumption, the total aerosol optical depth is the sum of optical depths of the individual components so that

$$\omega\tau_{total} = \tau_{sca} + \omega_{abs}\tau_{abs} \tag{3}$$

$$\tau_{total} = \tau_{sca} + \tau_{abs} \tag{4}$$

where again the subscript "sca" refers to the purely scattering aerosol component, "abs" refers to the absorbing aerosol, and ω is the single scattering albedo of the assemble of both aerosol types. For varying ω and fixed τ_{total}, the two equations above can be solved for the optical depth of the pure scattering aerosol τ_{sca}:

$$\tau_{sca} = \left(\frac{\omega - \omega_{abs}}{1 - \omega_{abs}}\right)\tau_{total} \tag{5}$$

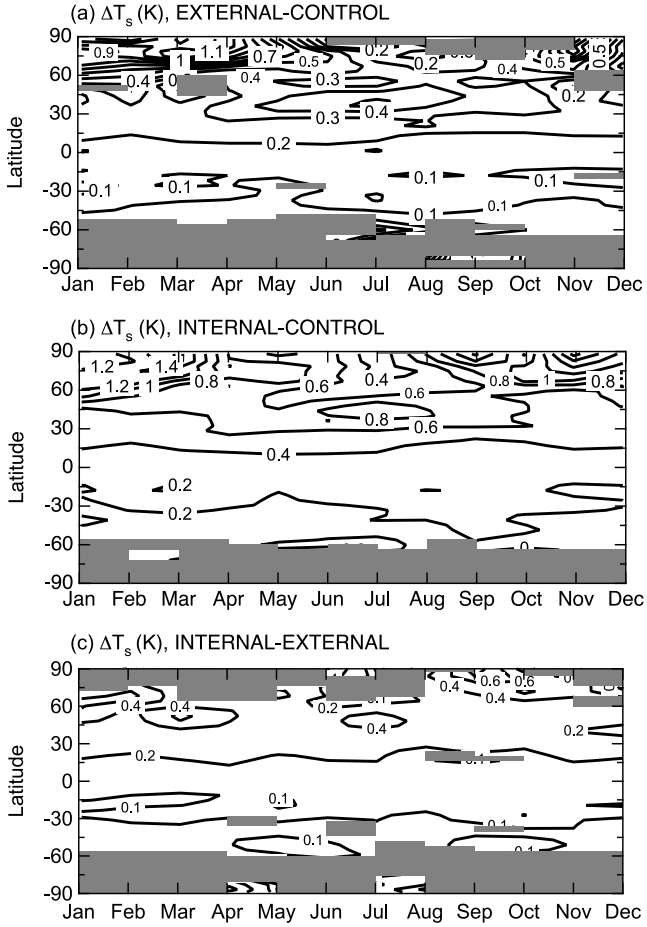

Figure 11. Estimated change in monthly and zonally averaged equilibrium surface air temperature (K) for (a) EXTERNAL minus CONTROL, (b) INTERNAL minus CONTROL, and (c) INTERNAL minus EXTERNAL. Gray indicates areas where the change is not significant at the 95% confidence level.

The radiative forcing contribution can also be separated into the purely scattering and absorbing components:

$$\Delta[\bar{F}] = \frac{\tau_{sca}}{\tau_{total}} \Delta\left[\bar{F}_{sca,\tau=\tau_{total}}\right] + \Delta[\bar{F}_{abs}] \quad (6)$$

The first term on the right accounts for the reduction in cooling due to the amount of purely scattering aerosol that is displaced by the absorbing aerosol, and the second term $\Delta[\bar{F}_{abs}]$ accounts for the warming due to the addition of the absorbing aerosol. The equation above can be rearranged to solve for $\Delta[\bar{F}_{abs}]$:

$$\Delta[\bar{F}_{abs}] = \Delta[\bar{F}] - \frac{\tau_{sca}}{\tau_{total}} \Delta\left[\bar{F}_{sca,\tau=\tau_{total}}\right] \quad (7)$$

Combining equations (1), (2), and (6), the temperature response is

$$\Delta[\bar{T}_s] = \lambda_{sca}\left(\frac{\tau_{sca}}{\tau_{total}} \Delta\left[\bar{F}_{sca,\tau=\tau_{total}}\right]\right) + \lambda_{abs}\Delta F_{abs} \quad (8)$$

The climate sensitivity factor for absorbing aerosol λ_{abs} can be solved from the above equation:

$$\lambda_{abs} = \frac{\Delta[\bar{T}_s] - \lambda_{sca}\left(\frac{\tau_{sca}}{\tau_{total}} \Delta\left[\bar{F}_{sca,\tau=\tau_{total}}\right]\right)}{\Delta F_{abs}} \quad (9)$$

[41] The calculated values for λ_{abs} based on the results of *Hansen et al.* [1997] and *Cook and Highwood* [2004] are given in Table 3 for $\omega_{abs} = 0.38$, which is the value of the single scattering albedo used for BC in this study. The calculated values for λ_{abs} shown in Table 3 indicate that, for a given climate model and within the same globally uniform distribution in optical depth, the climate sensitivities vary by less than 15%. For ω_{abs} in the range of 0 to 0.7, the values of λ_{abs} vary by less than 20%, which is within the model uncertainty.

[42] To summarize, the results of *Hansen et al.* [1997] and *Cook and Highwood* [2004] and the calculated λ_{abs} indicate that the proportionality between global mean surface air temperature change and direct radiative forcing is nearly constant for aerosols with single scattering albedo less than ~0.7. In other words, linearity is true for direct radiative forcing of BC (of which ω is on the order of 0.4); the linear relationship does not hold for the combined forcing of a mixture of BC plus sulfate (of which the composite ω is on the order of 0.9 depending on the mass ratio of each component). This supports the results of this study that the climate sensitivity of BC itself is independent of the mixing state.

[43] A note of caution must be noted with regard to the value of λ or λ_{abs}. There are two issues concerning the proportionality constant: (1) whether it is the same among different species, and (2) whether it varies for the same species under different conditions. With regard to the first issue, as noted in section 3.1, the climate sensitivity of BC is ~30% less than that of CO_2, consistent with the results of *Roberts and Jones* [2004]. With regard to the second issue, the linearity of climate response of BC direct radiative forcing has only been shown for limited cases. In both *Hansen et al.* [1997] and *Cook and Highwood* [2004],

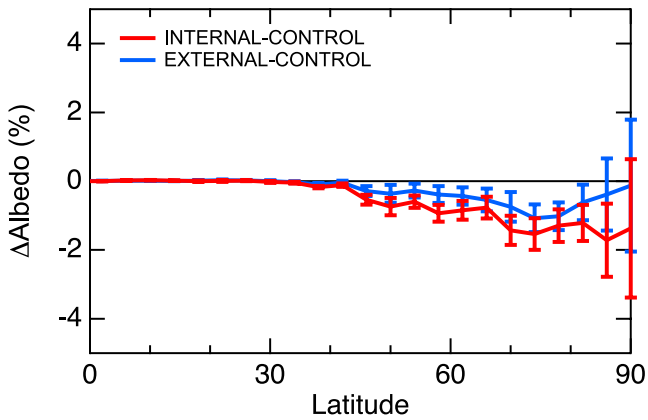

Figure 12. Estimated change in annually and zonally averaged surface albedo in the NH. The error bars indicate 95% confidence intervals.

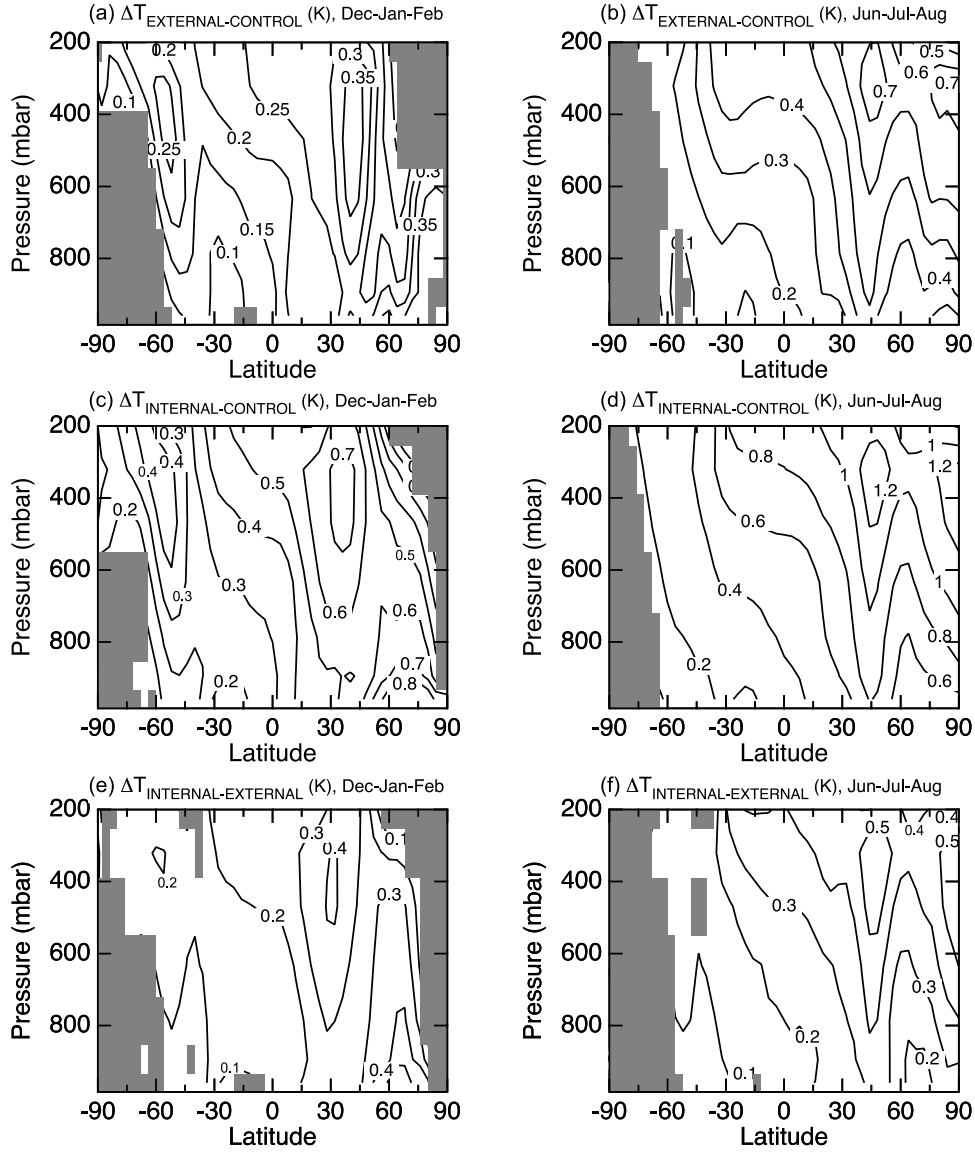

Figure 13. Estimated change in zonally averaged equilibrium temperature (K) as a function of pressure for December-January-February (left panel) and June-July-August (right panel) for EXTERNAL minus CONTROL (top panel), INTERNAL minus CONTROL (middle panel), and INTERNAL minus EXTERNAL (bottom panel). Gray indicates areas where the difference is not significant at the 95% confidence level.

optical depth is distributed uniformly throughout the globe. For this study, as direct radiative forcing of BC increases from being externally- to internally-mixed with sulfate, the distribution of the forcing remains mostly the same (with slight change due to the fact that the distribution of sulfate does not overlap completely with that of BC). The results of *Cook and Highwood* [2004] indicate that λ_{abs} is a factor of 2 higher for forcing located in the lower troposphere (695–930 mbar) in comparison to forcing located in the mid-troposphere (310–400 mbar), consistent with the ''ghost-forcing'' experiment of *Hansen et al.* [1997], in which arbitrary heating is added to the radiative source term in the energy equation. Also, note that in both *Hansen et al.* [1997] and *Cook and Highwood* [2004], for forcing in the lower troposphere, $\lambda_{abs} \sim 1.7\ \lambda_{2\times CO_2}$. The result of this study, i.e., $\lambda_{BC} \sim 0.7\lambda_{2\times CO_2}$, is similar to that of $\lambda_{abs} \sim 0.7\ \lambda_{2\times CO_2}$ calculated from the results of *Cook and Highwood* [2004] for forcing in the mid-troposphere. As mentioned previously in section 2.4.2 and indicated by Figure 6, maximum BC forcing is predicted to occur in the mid-troposphere. Clearly, the climate sensitivity of direct radiative forcing of BC is different if the vertical distribution of the forcing is different.

3.3. Monthly Mean Surface Air Temperature Response

[44] The monthly and zonally averaged surface air temperature response is shown in Figure 11. As *Hansen et al.* [1997] have shown, the equilibrium response of surface air temperature is insensitive to the seasonality of the forcing because the radiative relaxation time of the troposphere is on the order of months and the response time for mixed-

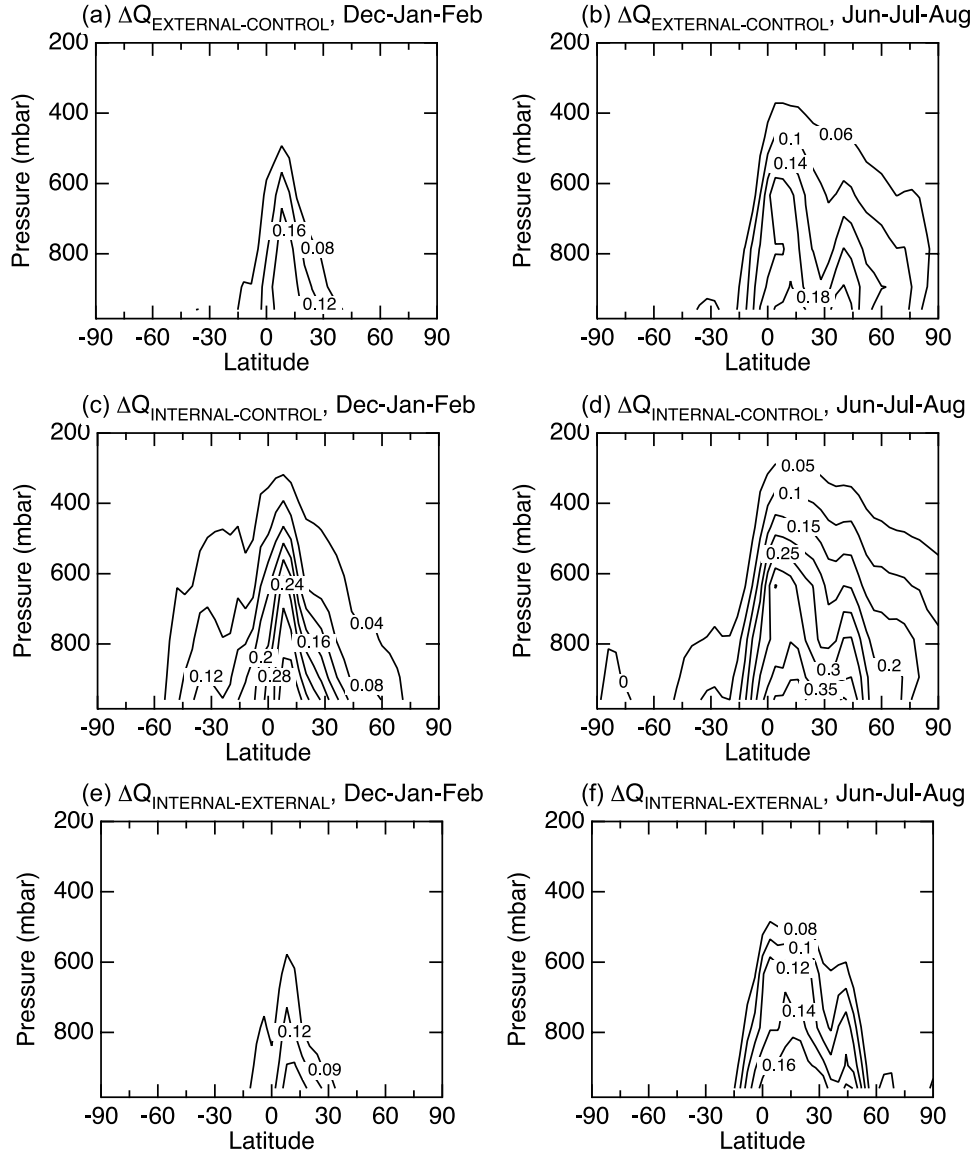

Figure 14. Estimated change in zonally averaged equilibrium specific humidity (g H_2O/kg air) as a function of pressure for December-January-February (left panel) and June-July-August (right panel) for EXTERNAL minus CONTROL (top panel), INTERNAL minus CONTROL (middle panel), and INTERNAL minus EXTERNAL (bottom panel). All nonzero contour lines indicate that the difference is significant at the 95% confidence level.

layer ocean is on the order of years. Figure 11 indicates that the greatest change in surface temperature in the northern high latitudes occurs during winter and early spring. At the northern midlatitudes, the warming is on the order of 0.3 K, with slightly more warming occurring during summer. In the tropics and southern midlatitudes, the surface air temperature is predicted to be less, on the order of 0.1 K, leading to an increase in the meridional temperature gradient between the northern and southern hemispheres. In contrast to the high latitudes, the response in the low and midlatitudes shows little seasonal variability. The surface response in the southern high latitudes is insignificant. In comparison to the externally-mixed case, internal mixing is predicted to extend the period of warming in the high northern latitudes and increase surface warming by around 0.3 K throughout the year in the midlatitudes and the tropics.

[45] Figures 8–11 reinforce previous studies on climate effects of CO_2, ozone, and solar forcings that the surface temperature response is the strongest in the high latitudes (in this case, the northern high latitudes). One reason, in the case of BC, is simply that the TOA radiative forcing is large in this region (see Figures 4 and 5). Another reason is that a forcing at high latitudes yields a stronger response than a forcing at low latitudes due to the positive feedback mechanism in which surface warming reduces snow and ice coverage, reducing surface albedo, and thus leading to even greater warming. The change in zonally averaged predicted annual mean surface albedo in the NH is shown in Figure 12. Also, at high latitudes during winter, a more

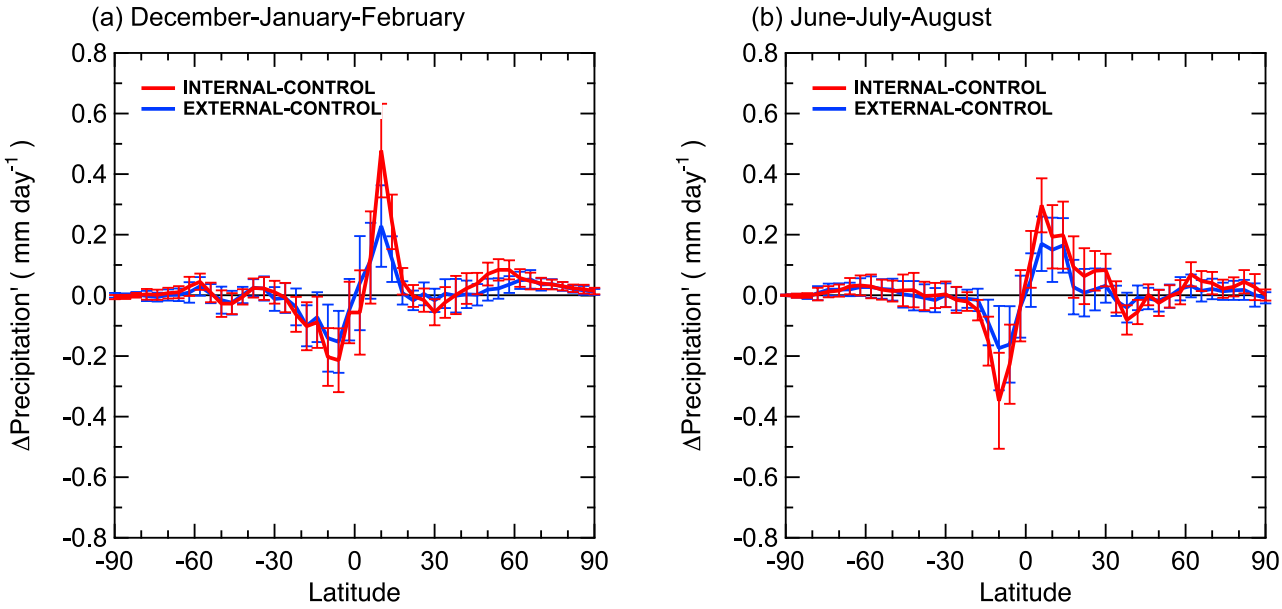

Figure 15. Estimated change in zonally averaged equilibrium precipitation rate (mm day^{-1}) for (a) December-January-February and (b) June-July-August. The error bars indicate 95% confidence intervals.

stable lapse rate tends to confine the thermal response close the the surface, as with the case of CO_2 suggested by *Manabe and Wetherald* [1975]. The positive albedo feedback mechanism and more stable lapse rate also causes the surface temperatures response to be the largest during winter even though TOA forcing is largest during spring and summer. Note that the reduced surface albedo in this study is the result of melting of ice and snow as BC direct radiative forcing warms the atmosphere and surface. The albedo change due to snow darkening effect studied in *Hansen and Nazarenko* [2004] and *Jacobson* [2004] is not considered here.

3.4. Vertical Distribution of Temperature Response

[46] The zonal mean temperature response as a function of pressure for DJF and JJA is shown in Figure 13. Warming is predicted to occur throughout most of the troposphere up to 200 mbar and north of 60°S. During JJA, the zonal and altitude pattern of the temperature response is similar to that of the forcing north of 30°N, otherwise the pattern of temperature response does not follow the pattern of forcing. As mentioned previously, high direct radiative forcing and ice-albedo feedback causes the warming to be largest in the northern high latitudes, and the stable lapse rate during northern winter tends to confine the temperature response close to the surface. During JJA, however, the largest temperature response occurs around 300 mbar in the northern polar region as well as around 45°N, close to the regions of the largest forcing at this time of the year. In the low and midlatitudes, the predicted warming is greatest in the the upper troposphere because moist convective processes tend to adjust temperatures in a column toward the moist adiabatic lapse rate, causing the maximum tropospheric warming to occur in the upper troposphere instead of near the surface [*Manabe and Wetherald*, 1975]. Even though forcing in the SH is small, substantial warming still occurs, especially around 60°S. The warming over the SH is partly a result of small radiative forcing but also because of dynamical and diffusion effects from warming in the NH. *Forster et al.* [2000] have shown that even when solar or CO_2 forcing is restricted to the NH (SH), substantial warming is predicted to occur in the SH (NH). Similarly, when *Chen and Ramaswamy* [1996b] perturb the climate by increasing liquid water path or reducing cloud droplet radius from 20° to 70°N, cooling is predicted in the SH. The results here further support the conclusion that local radiative forcing can cause climate change in remote regions. Overall, the predicted temperature increase of the internally-mixed case is almost twice that of the externally-mixed case.

3.5. Response of the Hydrological Cycle

[47] Figure 14 shows the predicted zonally averaged change in specific humidity as a function of pressure. Direct radiative forcing of BC causes an increase in water vapor in the atmosphere, consistent with increasing temperature. The water vapor mixing ratio increases most in the low latitudes and during JJA. As expected, the increase is greater if BC is assumed to be internally mixed with sulfate instead of externally mixed. Given that water vapor is a greenhouse gas, the increase in water vapor mixing ratio leads to a positive feedback loop on the temperature response.

[48] Another obvious change in the hydrological cycle is reflected in precipitation change, which is shown in Figure 15. BC radiative forcing is predicted to increase precipitation between 0 and 20°N and decrease precipitation between 0 and 20°S, effectively shifting the ITCZ northward. This result is similar to that predicted by *Roberts and Jones* [2004] and *Wang* [2004]. The greatest change occurs over the central Pacific, away from the location of largest BC forcing. The change in precipitation pattern can be explained by the enhanced interhemispheric temperature difference, which induces a change in the zonal mean meridional circulation and convection in the tropics.

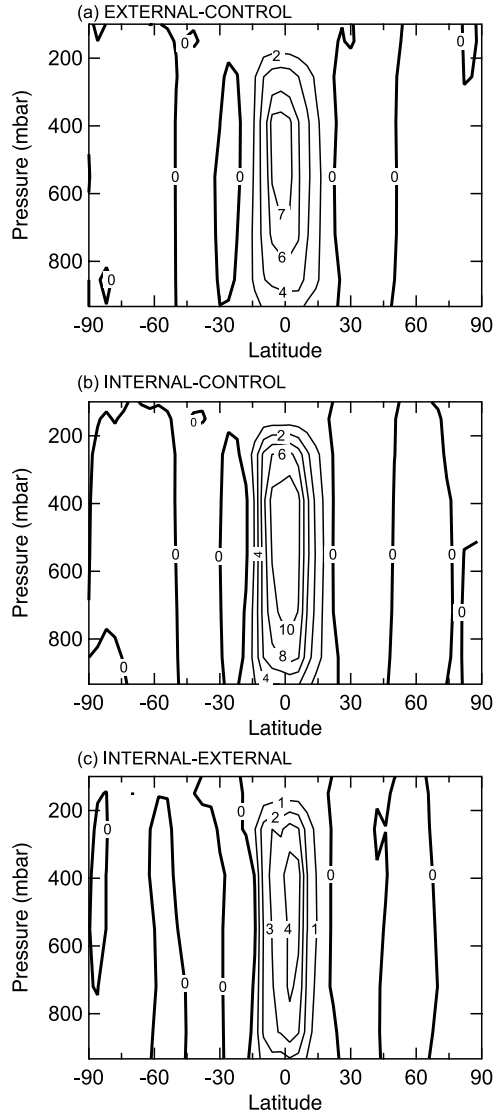

Figure 16. Estimated change in zonally and annually averaged mass stream function (10^9 kg s^{-1}) as a function of pressure. Positive values indicate anticlockwise circulation. All nonzero contour lines indicate that the difference is significant at the 95% confidence level.

Figure 16 shows the predicted change in annually and zonally averaged mass stream function. In the NH equatorial region, the ascending branch of the mean meridional circulation is enhanced, accompanied by a strong moisture flux convergence, leading to increased precipitation. Just south of the equator, the opposite is true: the ascending branch of the zonal mean meridional circulation is weakened, reducing precipitation. The change in the meridional circulation occurs both in winter and summer, i.e., the Hadley cell circulation is weakened during DJF and strengthened during JJA. Note that the predicted change in meridional flow and precipitation pattern is opposite to that of *Chen and Ramaswamy* [1996b], who studied the climate sensitivity to increased cloud liquid water path between 20°–70°N. In that study, increased cloud albedo in the NH leads to larger cooling in the NH than in the SH, leading to change in the meridional transport such that precipitation is increased south of the equator and reduced north of the equator.

[49] The change in precipitation pattern around the tropics correlates with change in convective cloud cover. Figure 17 shows the predicted zonal mean change in convective and large-scale cloud cover. The increase in precipitation between 0° to 20°N is matched closely by increased convective cloud cover; similarly, the decrease in precipitation between 0° and 20°S is accompanied by reduction in convective cloud cover. Note that even though BC direct radiative forcing is the greatest over the NH, the reduction in convective cloud cover in the SH is greater than the corresponding increase in the NH. For both convective cloud cover and precipitation, the largest response occurs during the winter months of each hemisphere. As seen from Figure 18, which shows the change in cloud cover for each hemisphere as a function of pressure, the change in cloud cover occurs predominately between 300 and 500 mbar. Similar to the temperature response, the impact of BC direct radiative forcing on cloud cover is greater in the case of internally-mixed BC than in the case of externally-mixed BC.

[50] In addition to change in convective cloud, direct radiative forcing of BC is also predicted to change large-scale cloud cover, which is shown in Figures 17 and 18. Around the equator, the change in large-scale clouds is similar to the change in convective clouds, again due to increased northward transport of water vapor across the equator near the surface, resulting in increased cloud cover in the northern equatorial region and reduction in cloud cover in the southern equatorial region. Because of radiative warming of BC in northern mid- and high latitudes, low and mid-level cloud covers are reduced, but high cloud cover is increased even more due to decreased static stability. This semi-direct effect of absorbing aerosol is also observed in the study of *Cook and Highwood* [2004] and is similar to the effect of the "ghost" forcing experiments of *Hansen et al.* [1997]. According to *Hansen et al.* [1997], for high clouds (above 7–8 km), the warming from the greenhouse effect of cloud water on globally averaged surface air temperature dominates the cooling from the cloud albedo effect. The competing cloud albedo and greenhouse effects are especially strong in the northern tropics, as seen in Figure 19, which shows the predicted change in zonal mean equilibrium shortwave and longwave radiative fluxes. In the northern tropics the increase in high level clouds reflects more solar radiation back to space such that the net solar radiation absorbed by the planet is negative even though the initial perturbation of direct radiative forcing is positive. The greenhouse effect of high clouds, i.e., increased downward longwave radiation, however, leads to net warming. In contrast to high clouds, for mid- and low level clouds, the albedo effect dominates the greenhouse effect. Therefore, the semi-direct effect of BC introduces a positive feedback on surface temperature increase by reducing low- and mid-level clouds and increasing high level clouds.

3.6. Change in Surface Energy Budget

[51] The climate response due to BC can be studied from the change in surface energy budget. Figure 20 shows the

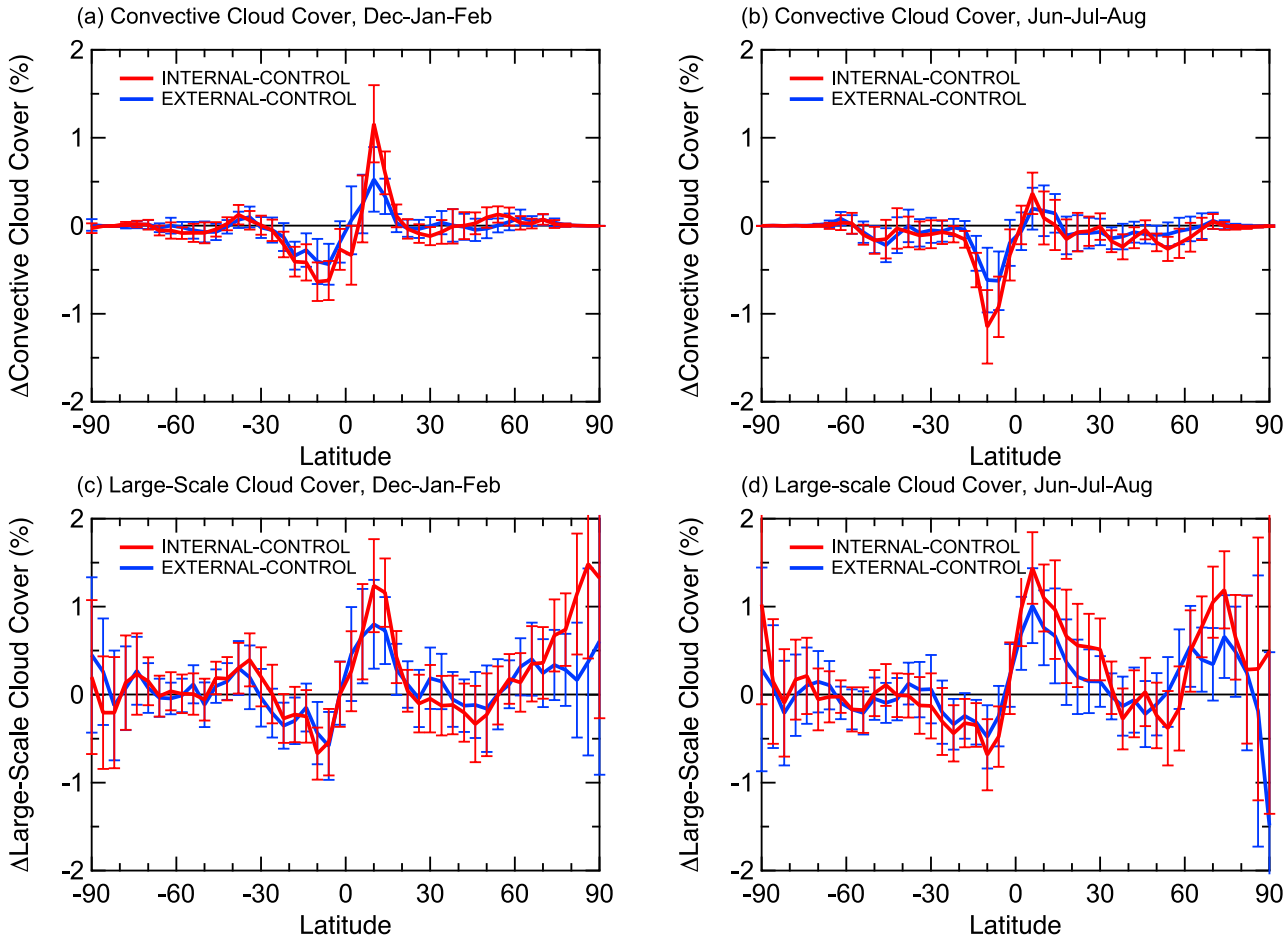

Figure 17. Estimated change in zonally averaged equilibrium cloud cover for December-January-February (left left panel) and June-July-August (right panel) for convective cloud (top panel) and large-scale cloud (bottom panel). The error bars indicate 95% confidence intervals.

zonal and annual mean change in surface energy fluxes. As expected, shortwave absorption by BC in the atmosphere leads to reduction in absorbed shortwave radiation at the surface in most latitudes. In the northern low latitudes, the reduction in absorbed solar radiation at the surface after the climate has reached equilibrium is even greater than the instantaneous direct forcing at the surface that led to the change in climate because increased high cloud cover (see section 3.5) reflected even more solar radiation away from the surface. In the northern high latitudes, solar absorption at the surface actually increases because of the reduction in surface albedo as result of decreased ocean ice coverage and snow depth (see Figure 12).

[52] The change in net solar radiation at the surface is compensated by the change in longwave radiation, sensible heat flux, and latent heat flux. Figure 20b indicates an increase in net downward longwave radiation. This change is attributed to increase in atmospheric temperature and increased emissivity of a more moist atmosphere. Similar to the change in longwave radiation, decrease in sensible heat flux from the ground to the atmosphere also acts to compensate for the reduction in solar radiation, as the air above the surface is warmed more than the surface. Finally, changes in evaporation result in change in latent heat fluxes, which also correspond to the changes in precipitation pattern discussed in section 3.5.

3.7. Black Carbon Distribution

[53] Given that wet-scavenging is the dominant sink for atmospheric BC, one would expect that the global BC distribution would be altered by the change in the hydrological cycle. Figure 21 shows the annually and zonally averaged change in BC burden. As discussed previously, in the tropics precipitation is predicted to increase just north of the equator and decrease just south of the equator. For the case of externally-mixed BC, the reduction in wet scavenging dominates, leading to a slightly increased annually-averaged BC burden around the tropics. In comparison to the case of externally-mixed BC, for the internally-mixed case, the increase in precipitation between 0° and 20°N is predicted to be greater than the reduction in precipitation between 0° and 20°S; consequently, the annually-averaged BC burden is predicted to increase between 0° and 20°S and remained unchanged between 0° and 20°N. North of 30°N, the change in BC burden is extremely small and only greater than the natural variability of the model when internally-mixed case with sulfate. Overall, the change in global

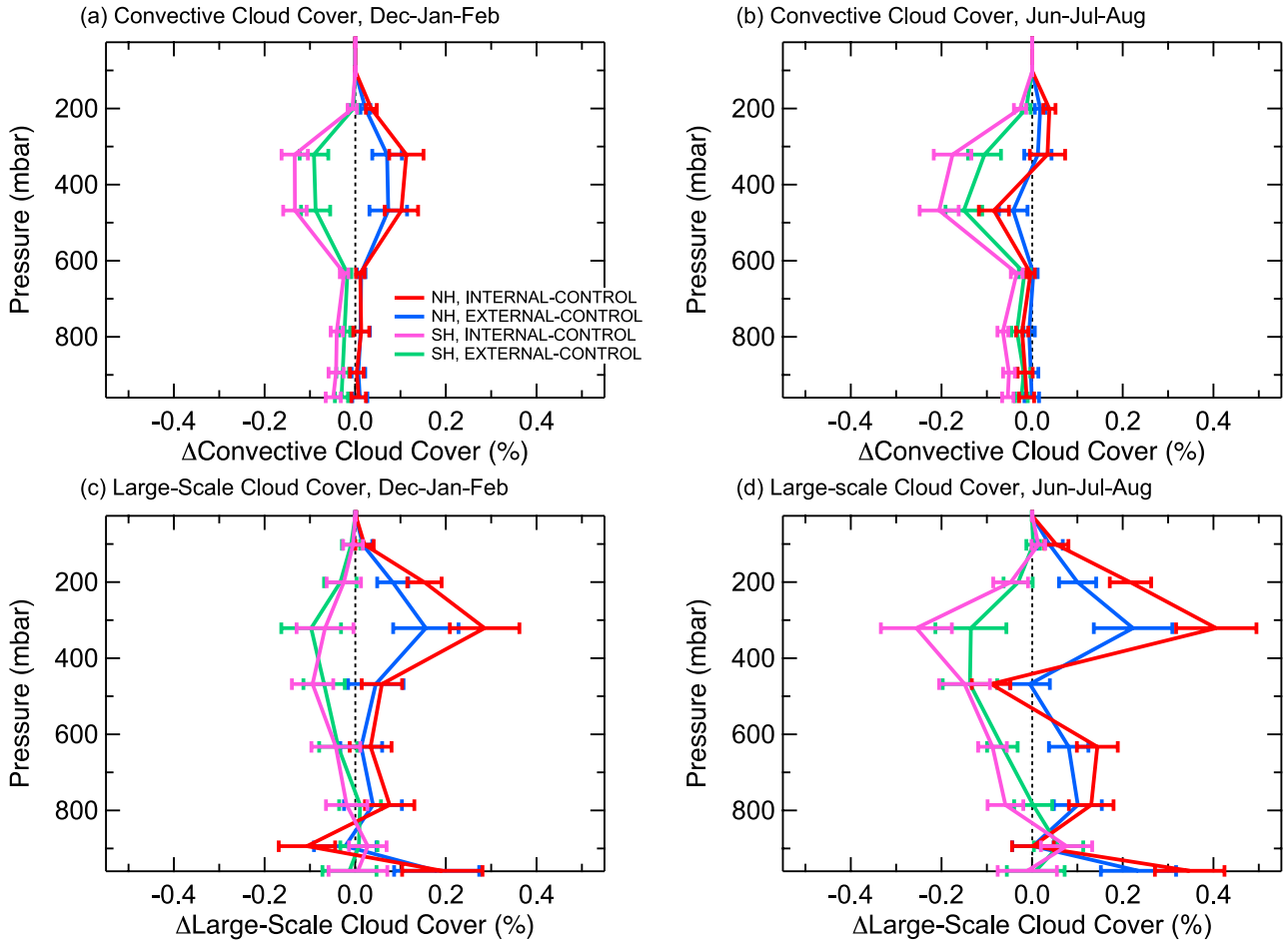

Figure 18. Estimated change in hemispherically averaged equilibrium cloud cover as a function of pressure for convective (top panel) and large-scale (bottom panel) clouds for December-January-February (left left panel) and June-July-August (right-panel). The error bars indicate 95% confidence intervals.

burden of BC is small (on the order of 0.5%) because the change in precipitation is predicted to occur mainly over oceans, away from regions of high BC concentrations.

4. Discussion of Uncertainties

[54] The results presented in the previous sections indicate that the climate response of BC is strongly dependent on the mixing state of BC with other aerosols. Given the prediction here that the climate sensitivity of BC radiative forcing is the same regardless of how BC is mixed with sulfate, at least in terms of global and annual mean surface temperature response, the results of this study provide upper and lower estimates for the climate impact of anthropogenic BC for this model. However, this study considers only BC and sulfate. In the real atmosphere, soot is emitted as a mixture of BC and OC such that all individual particles that contain BC also contain OC. Once emitted, these particles can also be mixed with other species via coagulation and condensation. When the amount of scattering material, such as nitrates or organic carbon, that is mixed with BC is increased, the absorbing efficiency of BC is enhanced even more [*Lesins et al.*, 2002], and BC has even greater climate impact.

[55] In addition to the mixing state of BC, other factors also contribute to uncertainties in the predicted direct radiative forcing of BC, which in turn leads to uncertainties of the climate response. Most importantly, direct radiative forcing of BC is strongly dependent on its global distribution. Unfortunately, constraining the model predictions of global BC distribution is difficult due to lack of long term data. The global burden and distribution of BC are most sensitive to the emission rate. *Bond et al.* [2004] suggest an uncertainty range for global BC emissions of 4.3 to 22 Tg yr^{-1}. Assuming radiative forcing scales linearly with emission rate and employing the climate sensitivity of 0.6 K W^{-1} m^2 determined here, the global and annual mean temperature increase attributed to anthropogenic BC is estimated to be between 0.11 and 1.0 K. In the northern polar region, the temperature increase is bracketed by 0.4 to 3.9 K. Even though the results presented here and from previous studies indicate that the zonal and global mean surface air temperature is, in some sense, independent of the distribution of forcing, regional impacts can still be important. For example, this study indicates anthropogenic BC leads to warming over central and eastern Russia that is not predicted for ozone or CO_2. This is likely a result of high emissions in the

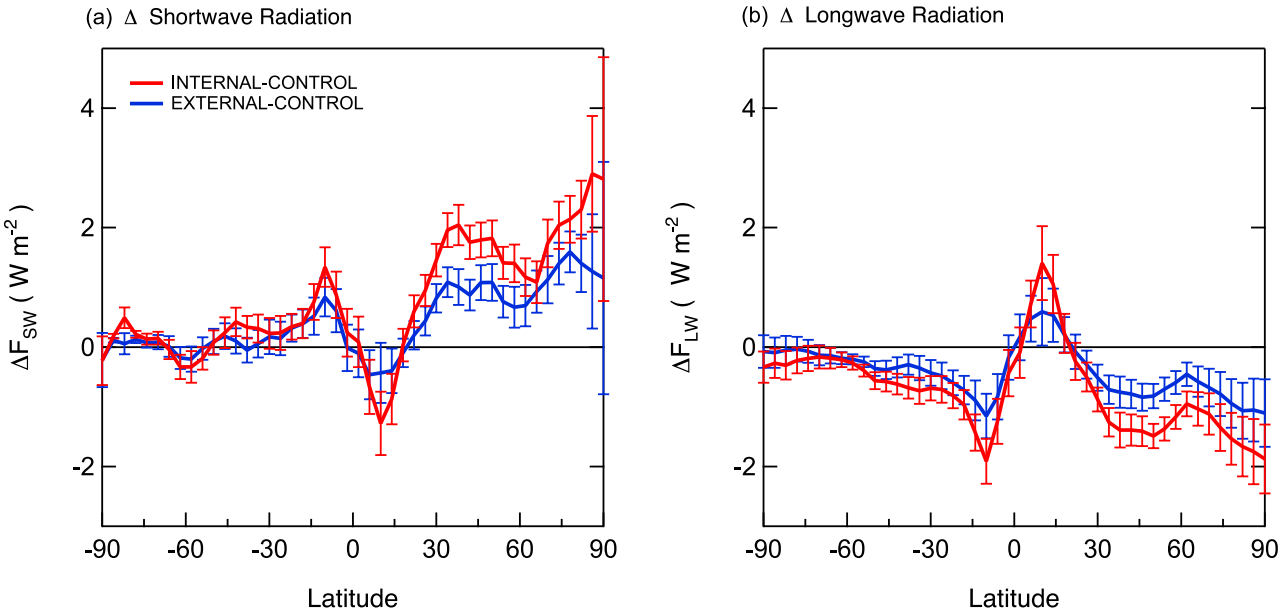

Figure 19. Estimated change in zonal mean equilibrium radiative flux of the planet for (a) shortwave radiation and (b) longwave radiation. A positive change indicates warming of the atmosphere. The error bars indicate 95% confidence intervals.

former USSR and China; however, in these regions uncertainties are large [*Bond et al.*, 2004].

[56] Another uncertainty is that in this study aerosol scavenging efficiency is treated as independent of the aerosol mixing state when in fact internally-mixed BC are more soluble in water and would be removed more efficiently from the atmosphere by wet deposition. In this study, the solubility of BC is determined by whether it is hydrophobic or hydrophilic (see section 2.3). The hydrophobic fraction of emitted BC is assumed to be 80% regardless of origin, burning characteristics, or meteorological conditions. Once emitted in the atmosphere, hydrophobic BC becomes hydrophilic with an e-folding lifetime of 1.15 days. Accurate modeling of solubility of BC would require knowledge of the morphology of BC particles and the rate at which they take up condensable gases such as H_2SO_4 and organics. *Cooke et al.* [2002] indicate that a factor of 2 uncertainty in the decay lifetime leads to approximately 20% uncertainty in global burden. In the extreme limit that all BC is emitted as hydrophilic aerosol, the global burden would be reduced by almost half. Overall, the physical and chemical properties of BC yield a factor of 2 uncertainty in the global burden and lifetime.

[57] Limitations of the climate model also make significant contribution to uncertainties in predicting climate response. One important issue is the coarse resolution of the model. According to *Rind and Lerner* [1996], finer vertical resolution in the GCM could lead to stronger convection and result in stronger coupling between the upper troposphere and the surface. Stronger convection would certainly be a factor in the change in the zonal mean precipitation pattern that is found in this study. A universal problem with all current GCMs is that the horizontal resolution does not resolve subgrid-scale cloud processes that could be important for BC-cloud interactions. Another factor is because in the climate model used for this study, the ocean ice albedo in the SH is set at a low value 0.25 to achieve a realistic ocean ice cover, climate response in the SH is dampened. Given that most of the forcing occurs in the NH and forcing is nearly zero southward of 60°S, the error introduced by the low SH ocean ice albedo is likely small. Finally, land-surface processes such as those affecting the distribution of water and thermodynamics of the boundary layer are another source of uncertainty in climate predictions.

5. Conclusions

[58] This study examines the interaction between BC and climate in a three-dimensional climate model. Three 100-year climate simulations are carried out, and the changes in equilibrium climate due to direct radiative forcing of anthropogenic BC are analyzed. Anthropogenic BC is predicted to raise global and annual mean surface air temperature by 0.20 to 0.37 K depending on whether BC is externally- or internally-mixed with the present-day level of sulfate aerosol, indicating that the mixing state of BC contributes to significant uncertainty in the temperature response. Over the northern high latitudes, the predicted surface air temperature increases by more than 1 K during winter and early spring. The large sensitivity at the high latitudes is a result of high surface albedo and positive feedback in which warming causes reduction in ice and snow cover, leading to reduced surface albedo and more absorbed solar radiation. Other than the northern high latitudes, substantial surface warming is predicted to also occur over most of Asia and the Atlantic and Pacific oceans. When BC is internally mixed with sulfate aerosol, the geographical extent of predicted surface warming covers the entire NH as well as parts of the SH. The results indicate that regional climate impacts of BC can be important, but not necessarily local to the place of maximum forcing. The

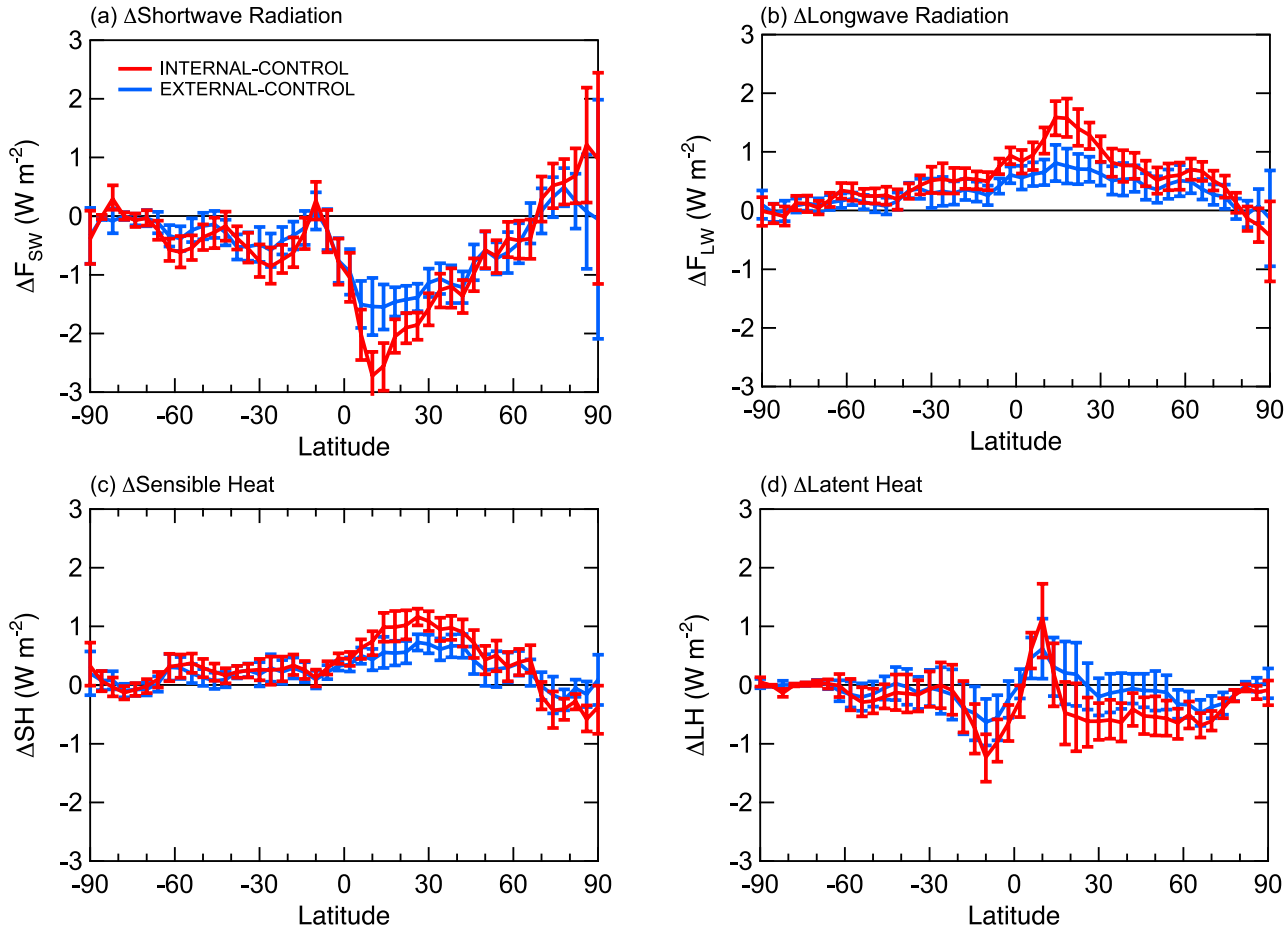

Figure 20. Estimated zonal and annual change (W m^{-2}) in (a) shortwave radiative flux, (b) longwave radiative flux, (c) sensible heat flux, and (d) latent heat flux at the the surface. A positive change indicates warming of the surface.

zonal mean pattern of surface response of BC direct radiative forcing is similar to that of ozone and CO_2 using the same GCM; however, significant warming is predicted for BC over central Russia but not for ozone or CO_2, suggesting that the regional climate impact of BC is different from that of ozone and CO_2. Other than at the surface, the temperature is predicted to increase throughout the troposphere, especially around 45°N and 400 mbar, which overlaps with the location of largest BC forcing. Over the tropics, the maximum warming occurs in the upper troposphere.

[59] In addition to the thermal response, direct radiative forcing of BC is also predicted to a change precipitation patterns in the tropics. Due to the change in the meridional temperature gradient between the northern and southern hemispheres, a change in the Hadley cell circulation leads to increased precipitation north of the equator and compensating reduction in precipitation south of the equator. Despite wet-scavenging being the dominant sink for atmospheric BC, the global distribution of BC is not expected to change significantly because the change in precipitation pattern tends to occur over the oceans, away from regions of high BC loading. The change in precipitation pattern away from the regions of largest BC forcing is one example of the complex nature of the climate response.

[60] For both externally- and internally-mixed BC, the predicted climate sensitivity of BC direct radiative forcing is estimated to be 0.6 K W^{-1} m^2, suggesting that a linear relationship between forcing and surface temperature response is valid for BC (i.e., equation (1)). The predicted

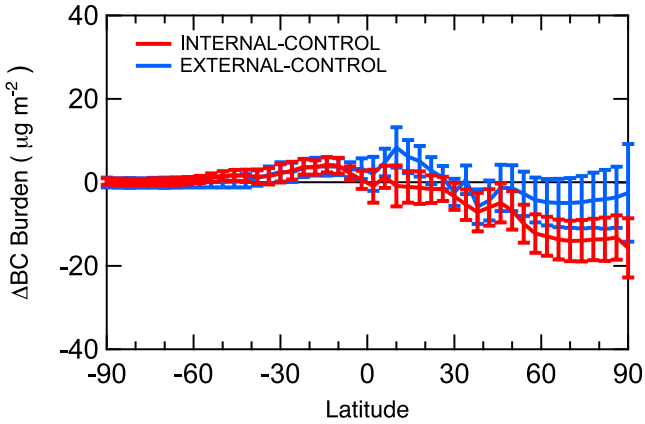

Figure 21. Estimated change in annually and zonally averaged BC column burden (μg m^{-2}). The error bars indicate 95% confidence intervals.

sensitivity is about 30% less than that of doubled CO_2 and similar to that of anthropogenic ozone forcing, all using the same climate model. Even though the predicted direct radiative forcing and climate sensitivity of anthropogenic BC are smaller than those of CO_2, regional differences in temperature and precipitation response still make climate impact of BC important. Overall, larger forcing for internally-mixed BC leads to greater climate response. The increase in temperature, changed precipitation pattern, and altered cloud coverage are all enhanced if BC is assumed to be internally mixed with sulfate instead of externally mixed. These results confirm that the mixing state of BC with other aerosols is important in determining its climate effect.

[61] **Acknowledgments.** This work was supported by the National Aeronautics and Space Administration Earth Observing System Interdisciplinary Science program (NASA EOS-IDS). Serena Chung was supported by a National Science Foundation Graduate Fellowship. The authors thank Loretta Mickley and Jean Lerner for assistance.

References

Adams, P. J., J. H. Seinfeld, and D. M. Koch (1999), Global concentrations of tropospheric sulfate, nitrate, and ammonium aerosol simulated in a general circulation model, *J. Geophys. Res.*, *104*, 13,791–13,823.

Adams, P. J., J. H. Seinfeld, D. M. Koch, L. Mickley, and D. Jacob (2001), General circulation model assessment of direct radiative forcing by sulfate-nitrate-ammonium-water inorganic aerosol system, *J. Geophys. Res.*, *106*(D1), 1097–1111.

Boer, G. J., and B. Yu (2003), Climate sensitivity and response, *Clim. Dyn.*, *20*(4), 415–429.

Bond, T. C., D. G. Streets, K. F. Yarber, S. M. Nelson, J. Woo, and Z. Klimont (2004), A technology-based global inventory of black and organic carbon emissions from combustion, *J. Geophys. Res.*, *109*, D14203, doi:10.1029/2003JD003697.

Chen, C.-T., and V. Ramaswamy (1996a), Sensitivity of simulated global climate to perturbations in low-cloud microphysical properties. part I: Globally uniform perturbations, *J. Clim.*, *9*, 1385–1402.

Chen, C.-T., and V. Ramaswamy (1996b), Sensitivity of simulated global climate to perturbations in low-cloud microphysical properties. part II: Localized perturbations, *J. Clim.*, *9*, 2788–2801.

Chung, S. H., and J. H. Seinfeld (2002), Global distribution and climate forcing of carbonaceous aerosols, *J. Geophys. Res.*, *107*(D19), 4407, doi:10.1029/2001JD001397.

Cook, J., and J. Highwood (2004), Climate response to tropospheric absorbing aerosols in an intermediate general-circulation model, *Q. J. R. Meteorol. Soc.*, *130*, 175–191.

Cooke, W. F., V. Ramaswamy, and P. Kasibhatla (2002), A general circulation model study of the global carbonaceous aerosol distribution, *J. Geophys. Res.*, *107*(D16), 4279, doi:10.1029/2001JD001274.

Cooke, W. F. C., C. Liousse, H. Cachier, and J. Feichter (1999), Construction of a $1^\circ \times 1^\circ$ fuel emission data set for carbonaceous aerosol and implementation and radiative impact in the ECHAM4 model, *J. Geophys. Res.*, *104*(D18), 22,137–22,162.

d'Almeida, G. A., P. Koepke, and E. P. Shettle (1991), *Atmospheric Aerosol: Global Climatology and Radiative Characteristsics*, A. Deepak, Hampton, Va.

Dana, M. T., and J. M. Hales (1976), Statistical aspects of the washout of polydispersed aerosols, *Atmos. Environ.*, *10*, 45–50.

Del Genio, A. D., and Y. Yao (1993), Efficient cumulus parameterization for long-term climate studies: The GISS scheme, in *The Representation of Cumulus Convection in Numerical Models*, *Monogr. 46*, edited by K. E. Emanuel and D. J. Raymond, pp. 181–184, Am. Meteorol. Soc., Boston, Mass.

Del Genio, A. D., M.-S. Yao, W. Kavari, and K. K.-W. Lo (1996), A prognostic cloud water parameterization for global climate models, *J. Clim.*, *9*, 270–304.

Forster, P., M. Blackburn, R. Glover, and K. Shine (2000), An examination of climate sensitivity for idealised climate change experiments in an intermediate general circulation model, *Clim. Dyn.*, *16*(10–11), 833–849.

Grégoire, J.-M., K. Tansey, and J. Silva (2003), The GBA2000 initiative: Developing a global burned area database from SPOT-VEGETATION imagery, *Int. J. Remote Sens.*, *24*(6), 1369–1376.

Hansen, J., and L. Nazarenko (2004), Soot climate forcing via snow and ice albedos, *Proc. Natl. Acad. Sci.*, *101*(2), 123–428, doi:10.1073/pnas.2237157100.

Hansen, J., G. Russell, D. Rind, P. Stone, A. Lacis, S. Lebedeff, R. Ruedy, and L. Travis (1983), Efficient three-dimensional global models for climate studies: Model I and II, *Mon. Weather Rev.*, *111*, 609–662.

Hansen, J., A. Lacis, G. Russell, P. Stone, I. Fung, R. Ruedy, and J. Lerner (1984), Climate sensitivity: Analysis of feedback mechanisms, in *Climate Processes and Climate Sensitivity*, *Geophys. Monogr. Ser.*, vol. 29, edited by J. E. Hansen and T. Takahashi, pp. 130–163, AGU, Washington, D. C.

Hansen, J., M. Sato, and R. Reudy (1997), Radiative forcing and climate response, *J. Geophys. Res.*, *102*(D6), 6831–6864.

Haywood, J. M., and V. Ramaswamy (1998), Global sensitivity studies of the direct forcing due to anthropogenic sulfate and black carbon aerosols, *J. Geophys. Res.*, *103*(D6), 6043–6058.

Haywood, J. M., and K. P. Shine (1995), The effect of anthropogenic sulfate and soot aerosol on the clear sky planetary radiation budget, *Geophys. Res. Lett.*, *22*, 603–605.

Haywood, J. M., D. L. Roberts, A. Slingo, J. M. Edwards, and K. P. Shine (1997), General circulation model calculations of the direct radiative forcing by anthropogenic sulfate and fossil-fuel soot aerosol, *J. Clim.*, *10*, 1562–1577.

Houghton, J. T., Y. Ding, D. J. Griggs, M. Noguer, P. J. van der Linden, D. Xiaosu, K. Maskell, and C. A. Johnson (Eds.) (2001), *Intergovernmental Panel on Climate Change, Climate Change 2001: The Scientific Basis*, Cambridge Univ. Press, New York.

Jacobson, M. Z. (2000), A physically-based treatment of elemental carbon optics: Implication for global direct forcing of aerosols, *Geophys. Res. Lett.*, *27*(2), 217–220.

Jacobson, M. Z. (2002), Control of fossil-fuel particulate black carbon and organic matter, possibly the most effective method of slowing global warming, *J. Geophys. Res.*, *107*(D19), 4410, doi:10.1029/2001JD001376.

Jacobson, M. Z. (2004), Climate response of fossil fuel and biofuel soot, accounting for soot's feedback to snow and sea ice albedo and emissivity, *J. Geophys. Res.*, *109*, D21201, doi:10.1029/2004JD004945.

Joshi, M., K. Shine, M. Ponater, N. Stuber, R. Sausen, and L. Li (2003), A comparison of climate response to different radiative forcings in three general circulation models: Toward an improved metric of climate change, *Clim. Dyn.*, *20*, 843–854, doi:10.1007/s00382-003-0305-9.

Koch, D. (2001), The transport and direct radiative forcing of carbonaceous and sulfate aerosols in the GISS GCM, *J. Geophys. Res.*, *106*(D17), 20,311–20,332.

Koch, D., D. Jacob, I. Tegen, D. Rind, and M. Chin (1999), Tropospheric sulfur simulation and sulfate direct radiative forcing in the Goddard Institute for Space Studies general circulation model, *J. Geophys. Res.*, *104*(D19), 23,799–23,822.

Lesins, G., P. Chýlek, and U. Lohmann (2002), A study of internal and external mixing scenarios ans its effect on aerosol optical properties and direct radiative forcing, *J. Geophys. Res.*, *107*(D10), 4094, doi:10.1029/2001JD000973.

Liousse, C., J. E. Penner, C. Chuang, J. J. Walton, H. Eddleman, and H. Cachier (1996), A global three-dimensional model study of carbonaceous aerosols, *J. Geophys. Res.*, *101*(D14), 19,411–19,432.

Manabe, S., and R. T. Wetherald (1975), The effects of doubling CO_2 concentration on the climate of a general circulation model, *J. Atmos. Sci.*, *32*(1), 3–15.

Markowicz, K. M., P. J. Flatau, M. V. Ramana, P. Crutzen, and V. Ramanathan (2002), Absorbing Mediterranean aerosols lead to a large reduction in the solar radiation at the surface, *Geophys. Res. Lett.*, *29*(20), 1968, doi:10.1029/2002GL015767.

Menon, S., J. Hansen, L. Nazarenkk, and Y. Lup (2002), Climate effects of black carbon aerosols in China and India, *Science*, *297*, 2250–2253.

Mickley, L. J., P. Murti, D. Jacob, J. Logan, D. Koch, and D. Rind (1999), Radiative forcing from tropospheric ozone calculated with a unified chemistry-climate model, *J. Geophys. Res.*, *104*, 30,135–30,172.

Mickley, L. J., D. J. Jacob, B. D. Field, and D. Rind (2004), Climate response to the increase in tropospheric ozone since preindustrial times: A comparison between ozone and equivalent CO_2 forcings, *J. Geophys. Res.*, *109*, D05106, doi:10.1029/2003JD003653.

Myhre, G., F. Stordal, K. Restad, and I. S. A. Isaksen (1998), Estimation of the direct radiative forcing due to sulfate and soot aerosols, *Tellus, Ser. B*, *50*, 463–477.

Nenes, A., C. Pilinis, and S. N. Pandis (1998), ISORROPIA: A new thermodynamics equilibrium model for multiphase multicomponent inorganic aerosols, *Aquat. Geochem.*, *4*, 23–152.

Penner, J. E., H. Eddleman, and T. Novakov (1993), Towards the development of a global inventory for black carbon emissions, *Atmos. Environ., Part A*, *27*, 1277–1295.

Penner, J. E., C. C. Chuang, and K. Grant (1998), Climate forcing by carbonaceous and sulfate aerosols, *Clim. Dyn.*, *14*, 839–851.

Ramanathan, V., P. J. Crutzen, J. T. Kiehl, and D. Rosenfeld (2001a), Aerosols, climate, and the hydrological cycle, *Science*, *294*(5549), 2119–2124.

Ramanathan, V., et al. (2001b), Indian Ocean Experiment: An integrated analysis of the climate forcing and effects of the great Indo-Asian haze, *J. Geophys. Res.*, *106*(D22), 28,371–28,398.

Rind, D., and J. Lerner (1996), Use of on-line tracers as a diagnostic tool in general circulation model development: 1. Horizontal and vertical transport in the troposphere, *J. Geophys. Res.*, *101*, 12,667–12,683.

Roberts, D. L., and A. Jones (2004), Climate sensitivity to black carbon aerosol from fossil fuel combustion, *J. Geophys. Res.*, *109*, D16202, doi:10.1029/2004JD004676.

Russell, G. L., J. R. Miller, and L.-C. Tsang (1984), Seasonal ocean heat transports computed from an atmospheric model, *Dyn. Atmos. Oceans*, *9*, 253–271.

Shine, K. P., and P. Forster (1999), The effect of human activity on radiative forcing of climate change: A review of recent developments, *Global Planet. Change*, *20*, 205–225.

Tegen, I., D. Koch, A. A. Lacis, and M. Sato (2000), Trends in tropospheric aerosol loads and corresponding impact on direct radiative forcing between 1950 and 1990: A model study, *J. Geophys. Res.*, *105*(D22), 26,971–26,989.

Toon, O. B., J. B. Pollack, and B. N. Khare (1976), The optical constants of several atmospheric aerosol species: Ammonium sulfate, aluminum oxide, and sodium chloride, *J. Geophys. Res.*, *81*, 5733–5748.

Wang, C. (2004), A modeling study on the climate impact of black carbon aerosols, *J. Geophys. Res.*, *109*, D03106, doi:10.1029/2003JD004084.

Zwiers, F. W., and H. von Storch (1995), Taking serial correlation into account in tests of the mean, *J. Clim.*, *8*, 336–351.

S. H. Chung, Aeronomy Laboratory, NOAA, 325 Broadway, R/AL 4, Boulder, CO 80305, USA. (serena.chung@noaa.gov)

J. H. Seinfeld, Department of Chemical Engineering, California Institute of Technology, Pasadena, CA 91125, USA. (seinfeld@caltech.edu)